

Searching for neutrinos from solar flares across solar cycles 23 and 24 with the Super-Kamiokande detector

K. OKAMOTO,¹ K. ABE,^{1,47} Y. HAYATO,^{1,47} K. HIRAIDE,^{1,47} K. HOSOKAWA,¹ K. IEKI,¹ M. IKEDA,¹
J. KAMEDA,^{1,47} Y. KANEMURA,¹ Y. KANESHIMA,¹ Y. KATAOKA,¹ Y. KASHIWAGI,¹ S. MIKI,¹
S. MINE,^{1,7} M. MIURA,^{1,47} S. MORIYAMA,^{1,47} Y. NAGAO,¹ M. NAKAHATA,^{1,47} Y. NAKANO,¹
S. NAKAYAMA,^{1,47} Y. NOGUCHI,¹ K. SATO,¹ H. SEKIYA,^{1,47} K. SHIMIZU,¹ M. SHIOZAWA,^{1,47}
H. SHIBA,¹ Y. SONODA,¹ Y. SUZUKI,¹ A. TAKEDA,^{1,47} Y. TAKEMOTO,¹ A. TAKENAKA,¹ H. TANAKA,¹
S. WATANABE,¹ T. YANO,¹ S. HAN,² T. KAJITA,^{2,47,23} K. OKUMURA,^{2,47} T. TASHIRO,² T. TOMIYA,²
X. WANG,² J. XIA,² S. YOSHIDA,² G.D. MEGIAS,³ P. FERNANDEZ,⁴ L. LABARGA,⁴ N. OSPINA,⁴
B. ZALDIVAR,⁴ B.W. POINTON,^{6,51} E. KEARNS,^{5,47} J.L. RAAF,⁵ L. WAN,⁵ T. WESTER,⁵ J. BIAN,⁷
N.J. GRISKEVICH,⁷ W.R. KROPP,^{7,*} S. LOCKE,⁷ M. B. SMY,^{7,47} H.W. SOBEL,^{7,47}
V. TAKHISTOV,^{7,47,25} A. YANKELEVICH,⁷ J. HILL,⁸ J.Y. KIM,⁹ S.H. LEE,⁹ I.T. LIM,⁹ D.H. MOON,⁹
R.G. PARK,⁹ B. BODUR,¹⁰ K. SCHOLBERG,^{10,47} C.W. WALTER,^{10,47} A. BEAUCHÊNE,¹¹
L. BERNARD,¹¹ A. COFFANI,¹¹ O. DRAPIER,¹¹ S. EL HEDRI,¹¹ A. GIAMPAOLO,¹¹ TH.A. MUELLER,¹¹
A.D. SANTOS,¹¹ P. PAGANINI,¹¹ B. QUILAIN,¹¹ T. ISHIZUKA,¹² T. NAKAMURA,¹³ J.S. JANG,¹⁴
J.G. LEARNED,¹⁵ K. CHOI,¹⁶ S. CAO,¹⁷ L.H.V. ANTHONY,¹⁸ D. MARTIN,¹⁸ M. SCOTT,¹⁸
A.A. SZTUC,¹⁸ Y. UCHIDA,¹⁸ V. BERARDI,¹⁹ M.G. CATANESI,¹⁹ E. RADICIONI,¹⁹ N.F. CALABRIA,²⁰
L.N. MACHADO,²⁰ G. DE ROSA,²⁰ G. COLLAZUOL,²¹ F. IACOB,²¹ M. LAMOUREUX,²¹
M. MATTIAZZI,²¹ L. LUDOVICI,²² M. GONIN,²³ G. PRONOST,²³ C. FUJISAWA,²⁴ Y. MAEKAWA,²⁴
Y. NISHIMURA,²⁴ M. FRIEND,²⁵ T. HASEGAWA,²⁵ T. ISHIDA,²⁵ T. KOBAYASHI,²⁵ M. JAKKAPU,²⁵
T. MATSUBARA,²⁵ T. NAKADAIRA,²⁵ K. NAKAMURA,^{25,47} Y. OYAMA,²⁵ K. SAKASHITA,²⁵
T. SEKIGUCHI,²⁵ T. TSUKAMOTO,²⁵ N. BHUIYAN,²⁶ T. BOSCHI,²⁶ G.T. BURTON,²⁶ F. DI LODOVICO,²⁶
J. GAO,²⁶ A. GOLDSACK,²⁶ T. KATORI,²⁶ J. MIGENDA,²⁶ M. TAANI,²⁶ Z. XIE,²⁶ S. ZSOLDOS,²⁶
Y. KOTSAR,²⁷ H. OZAKI,²⁷ A.T. SUZUKI,²⁷ Y. TAKEUCHI,^{27,47} S. YAMAMOTO,²⁷ C. BRONNER,²⁸
J. FENG,²⁸ T. KIKAWA,²⁸ M. MORI,²⁸ T. NAKAYA,^{28,47} R.A. WENDELL,^{28,47} K. YASUTOME,²⁸
S.J. JENKINS,²⁹ N. MCCAULEY,²⁹ P. MEHTA,²⁹ A. TARRANT,²⁹ K.M. TSUI,²⁹ Y. FUKUDA,³⁰
Y. ITOW,^{31,32} H. MENJO,³¹ K. NINOMIYA,³¹ J. LAGODA,³³ S.M. LAKSHMI,³³ M. MANDAL,³³
P. MIJAKOWSKI,³³ Y.S. PRABHU,³³ J. ZALIPSKA,³³ M. JIA,³⁴ J. JIANG,³⁴ C.K. JUNG,³⁴ C. VILELA,³⁴
M.J. WILKING,³⁴ C. YANAGISAWA,^{34,†} M. HARADA,³⁵ H. ISHINO,³⁵ S. ITO,³⁵ H. KITAGAWA,³⁵
Y. KOSHIO,^{35,47} W. MA,³⁵ F. NAKANISHI,³⁵ N. PIPLANI,³⁵ S. SAKAI,³⁵ G. BARR,³⁶ D. BARROW,³⁶
L. COOK,^{36,47} S. SAMANI,³⁶ D. WARK,^{36,41} A. HOLIN,³⁷ F. NOVA,³⁷ J.Y. YANG,³⁸ J.E.P. FANNON,³⁹
M. MALEK,³⁹ J.M. MCELWEE,³⁹ O. STONE,³⁹ M.D. THIESSE,³⁹ L.F. THOMPSON,³⁹ H. OKAZAWA,⁴⁰
S.B. KIM,⁴² E. KWON,⁴² J.W. SEO,⁴² I. YU,⁴² A.K. ICHIKAWA,⁴³ K.D. NAKAMURA,⁴³
S. TAIRAFUNE,⁴³ K. NISHIJIMA,⁴⁴ M. KOSHIBA,^{45,*} K. IWAMOTO,⁴⁶ K. NAKAGIRI,⁴⁶ Y. NAKAJIMA,⁴⁶
S. SHIMA,⁴⁶ N. TANIUCHI,⁴⁶ M. YOKOYAMA,^{46,47} K. MARTENS,⁴⁷ P. DE PERIO,⁴⁷ M.R. VAGINS,^{47,7}
M. KUZE,⁴⁸ S. IZUMIYAMA,⁴⁸ M. INOMOTO,⁴⁹ M. ISHITSUKA,⁴⁹ H. ITO,⁴⁹ T. KINOSHITA,⁴⁹
R. MATSUMOTO,⁴⁹ Y. OMMURA,⁴⁹ N. SHIGETA,⁴⁹ M. SHINOKI,⁴⁹ T. SUGANUMA,⁴⁹ K. YAMAUCHI,⁴⁹
J.F. MARTIN,⁵⁰ H.A. TANAKA,⁵⁰ T. TOWSTEGO,⁵⁰ R. AKUTSU,⁵¹ R. GAUR,⁵¹
V. GOUSY-LEBLANC,^{51,‡} M. HARTZ,⁵¹ A. KONAKA,⁵¹ X. LI,⁵¹ N.W. PROUSE,⁵¹ S. CHEN,⁵²
B.D. XU,⁵² B. ZHANG,⁵² M. POSIADALA-ZEZULA,⁵³ S.B. BOYD,⁵⁴ D. HADLEY,⁵⁴ M. NICHOLSON,⁵⁴
M. O'FLAHERTY,⁵⁴ B. RICHARDS,⁵⁴ A. ALI,^{55,51} B. JAMIESON,⁵⁵ J. WALKER,⁵⁵ LL. MARTI,⁵⁶
A. MINAMINO,⁵⁶ G. PINTAUDI,⁵⁶ S. SANO,⁵⁶ R. SASAKI,⁵⁶ S. SUZUKI,⁵⁶ AND K. WADA⁵⁶

THE SUPER-KAMIOKANDE COLLABORATION

¹Kamioka Observatory, Institute for Cosmic Ray Research, University of Tokyo, Kamioka, Gifu 506-1205, Japan

- ²*Research Center for Cosmic Neutrinos, Institute for Cosmic Ray Research, University of Tokyo, Kashiwa, Chiba 277-8582, Japan*
- ³*Institute for Cosmic Ray Research, University of Tokyo, Kashiwa, Chiba 277-8582, Japan*
- ⁴*Department of Theoretical Physics, University Autonoma Madrid, 28049 Madrid, Spain*
- ⁵*Department of Physics, Boston University, Boston, MA 02215, USA*
- ⁶*Department of Physics, British Columbia Institute of Technology, Burnaby, BC, V5G 3H2, Canada*
- ⁷*Department of Physics and Astronomy, University of California, Irvine, Irvine, CA 92697-4575, USA*
- ⁸*Department of Physics, California State University, Dominguez Hills, Carson, CA 90747, USA*
- ⁹*Institute for Universe and Elementary Particles, Chonnam National University, Gwangju 61186, Korea*
- ¹⁰*Department of Physics, Duke University, Durham NC 27708, USA*
- ¹¹*Ecole Polytechnique, IN2P3-CNRS, Laboratoire Leprince-Ringuet, F-91120 Palaiseau, France*
- ¹²*Junior College, Fukuoka Institute of Technology, Fukuoka, Fukuoka 811-0295, Japan*
- ¹³*Department of Physics, Gifu University, Gifu, Gifu 501-1193, Japan*
- ¹⁴*GIST College, Gwangju Institute of Science and Technology, Gwangju 500-712, Korea*
- ¹⁵*Department of Physics and Astronomy, University of Hawaii, Honolulu, HI 96822, USA*
- ¹⁶*Institute for Basic Science (IBS), Daejeon, 34126, Korea*
- ¹⁷*Institute For Interdisciplinary Research in Science and Education, ICISE, Quy Nhon, 55121, Vietnam*
- ¹⁸*Department of Physics, Imperial College London, London, SW7 2AZ, United Kingdom*
- ¹⁹*Dipartimento Interuniversitario di Fisica, INFN Sezione di Bari and Università e Politecnico di Bari, I-70125, Bari, Italy*
- ²⁰*Dipartimento di Fisica, INFN Sezione di Napoli and Università di Napoli, I-80126, Napoli, Italy*
- ²¹*Dipartimento di Fisica, INFN Sezione di Padova and Università di Padova, I-35131, Padova, Italy*
- ²²*INFN Sezione di Roma and Università di Roma "La Sapienza", I-00185, Roma, Italy*
- ²³*ILANCE, CNRS, University of Tokyo International Research Laboratory, Kashiwa, Chiba 277-8582, Japan*
- ²⁴*Department of Physics, Keio University, Yokohama, Kanagawa, 223-8522, Japan*
- ²⁵*High Energy Accelerator Research Organization (KEK), Tsukuba, Ibaraki 305-0801, Japan*
- ²⁶*Department of Physics, King's College London, London, WC2R 2LS, UK*
- ²⁷*Department of Physics, Kobe University, Kobe, Hyogo 657-8501, Japan*
- ²⁸*Department of Physics, Kyoto University, Kyoto, Kyoto 606-8502, Japan*
- ²⁹*Department of Physics, University of Liverpool, Liverpool, L69 7ZE, United Kingdom*
- ³⁰*Department of Physics, Miyagi University of Education, Sendai, Miyagi 980-0845, Japan*
- ³¹*Institute for Space-Earth Environmental Research, Nagoya University, Nagoya, Aichi 464-8602, Japan*
- ³²*Kobayashi-Maskawa Institute for the Origin of Particles and the Universe, Nagoya University, Nagoya, Aichi 464-8602, Japan*
- ³³*National Centre For Nuclear Research, 02-093 Warsaw, Poland*
- ³⁴*Department of Physics and Astronomy, State University of New York at Stony Brook, NY 11794-3800, USA*
- ³⁵*Department of Physics, Okayama University, Okayama, Okayama 700-8530, Japan*
- ³⁶*Department of Physics, Oxford University, Oxford, OX1 3PU, United Kingdom*
- ³⁷*Rutherford Appleton Laboratory, Harwell, Oxford, OX11 0QX, UK*
- ³⁸*Department of Physics, Seoul National University, Seoul 151-742, Korea*
- ³⁹*Department of Physics and Astronomy, University of Sheffield, S3 7RH, Sheffield, United Kingdom*
- ⁴⁰*Department of Informatics in Social Welfare, Shizuoka University of Welfare, Yaizu, Shizuoka, 425-8611, Japan*
- ⁴¹*STFC, Rutherford Appleton Laboratory, Harwell Oxford, and Daresbury Laboratory, Warrington, OX11 0QX, United Kingdom*
- ⁴²*Department of Physics, Sungkyunkwan University, Suwon 440-746, Korea*
- ⁴³*Department of Physics, Faculty of Science, Tohoku University, Sendai, Miyagi, 980-8578, Japan*
- ⁴⁴*Department of Physics, Tokai University, Hiratsuka, Kanagawa 259-1292, Japan*

⁴⁵*The University of Tokyo, Bunkyo, Tokyo 113-0033, Japan*

⁴⁶*Department of Physics, University of Tokyo, Bunkyo, Tokyo 113-0033, Japan*

⁴⁷*Kavli Institute for the Physics and Mathematics of the Universe (WPI), The University of Tokyo Institutes for Advanced Study, University of Tokyo, Kashiwa, Chiba 277-8583, Japan*

⁴⁸*Department of Physics, Tokyo Institute of Technology, Meguro, Tokyo 152-8551, Japan*

⁴⁹*Department of Physics, Faculty of Science and Technology, Tokyo University of Science, Noda, Chiba 278-8510, Japan*

⁵⁰*Department of Physics, University of Toronto, ON, M5S 1A7, Canada*

⁵¹*TRIUMF, 4004 Wesbrook Mall, Vancouver, BC, V6T2A3, Canada*

⁵²*Department of Engineering Physics, Tsinghua University, Beijing, 100084, China*

⁵³*Faculty of Physics, University of Warsaw, Warsaw, 02-093, Poland*

⁵⁴*Department of Physics, University of Warwick, Coventry, CV4 7AL, UK*

⁵⁵*Department of Physics, University of Winnipeg, MB R3J 3L8, Canada*

⁵⁶*Department of Physics, Yokohama National University, Yokohama, Kanagawa, 240-8501, Japan*

ABSTRACT

Neutrinos associated with solar flares (solar-flare neutrinos) provide information on particle acceleration mechanisms during the impulsive phase of solar flares. We searched using the Super-Kamiokande detector for neutrinos from solar flares that occurred during solar cycles 23 and 24, including the largest solar flare (X28.0) on November 4th, 2003. In order to minimize the background rate we searched for neutrino interactions within narrow time windows coincident with γ -rays and soft X-rays recorded by satellites. In addition, we performed the first attempt to search for solar-flare neutrinos from solar flares on the invisible side of the Sun by using the emission time of coronal mass ejections (CMEs). By selecting twenty powerful solar flares above X5.0 on the visible side and eight CMEs whose emission speed exceeds 2000 km s^{-1} on the invisible side from 1996 to 2018, we found two (six) neutrino events coincident with solar flares occurring on the visible (invisible) side of the Sun, with a typical background rate of 0.10 (0.62) events per flare in the MeV–GeV energy range. No significant solar-flare neutrino signal above the estimated background rate was observed. As a result we set the following upper limit on neutrino fluence at the Earth $\Phi < 1.1 \times 10^6 \text{ cm}^{-2}$ at the 90% confidence level for the largest solar flare. The resulting fluence limits allow us to constrain some of the theoretical models for solar-flare neutrino emission.

Keywords: Neutrino astronomy (1100) — Solar flares (1496) — Particle astrophysics (96) — Solar energetic particles (1491)

1. INTRODUCTION

Solar flares are the largest explosive events that occur around the surface of the Sun. This phenomenon is caused by the reconnection of magnetic field lines above sun spots and produces electromagnetic radiation from radio to γ -rays (Kane 1974). Solar flares sometimes occur associated with

* Deceased.

† also at BMCC/CUNY, Science Department, New York, New York, 1007, USA.

‡ also at University of Victoria, Department of Physics and Astronomy, PO Box 1700 STN CSC, Victoria, BC V8W 2Y2, Canada.

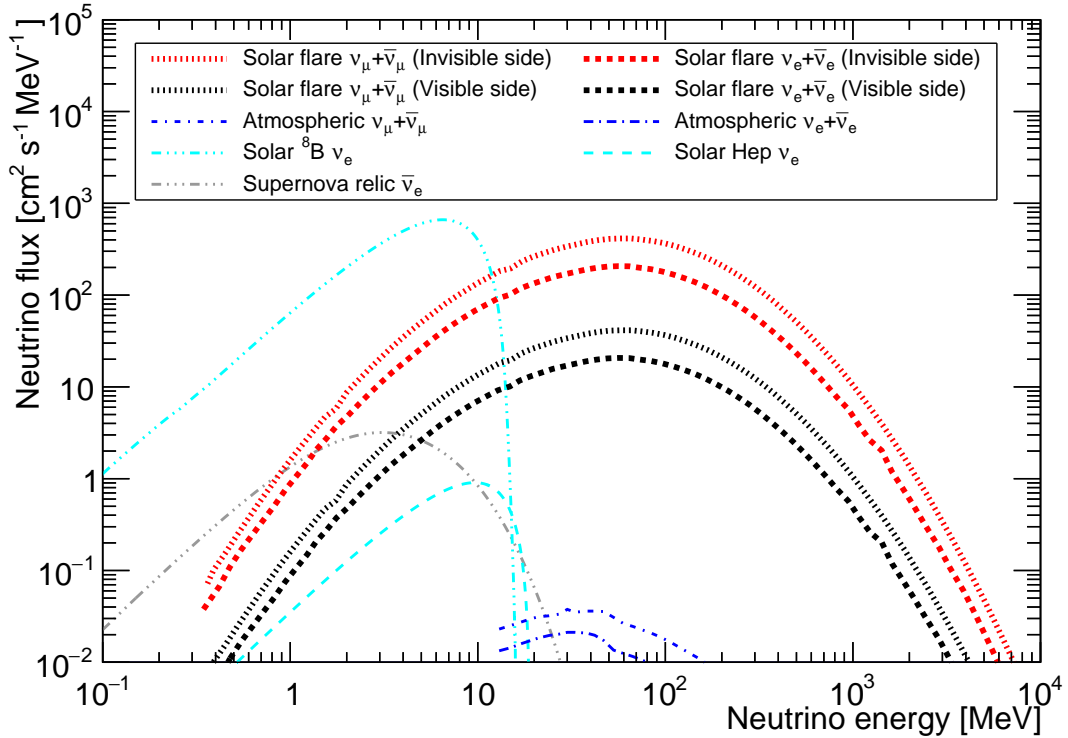


Figure 1. Typical solar-flare neutrino fluxes from a powerful solar flare (Fargion & Moscato (2003), red thick and black thick lines) together with other neutrino fluxes, such as atmospheric neutrinos (Battistoni et al. (2005), blue lines), solar neutrinos (Bahcall et al. (2001), light blue lines), and relic neutrinos (Horiuchi et al. (2009), light gray line).

coronal mass ejections (CMEs), which are eruptions of the atmospheric plasma into interplanetary space (Chao & Lepping 1974; Gosling et al. 1975). The frequency of these explosive events is strongly correlated with the activity of the Sun.

For both types of energetic events, the typical energy released by the explosion is estimated in the range of 10^{27} – 10^{32} erg (Ellison 1963; Hundhausen et al. 1994; Vourlidas et al. 2010). When a solar flare occurs, high energy particles that do not normally exist in the solar atmosphere are generated (Chupp et al. 1973; Datlowe et al. 1974). Solar imaging methods can partially identify the location at which these particles are generated, such as the magnetic loop-top (Masuda et al. 1994; Krucker et al. 2010), the loop-foot (Fletcher & Hudson 2008), and the reconnection point (Narukage et al. 2014). This indicates that these particles are accelerated by solar flares. Although the acceleration mechanisms remain poorly understood, several theoretical models of solar flares are proposed (Tsuneta & Naito 1998; Karlický & Kosugi 2004; Liu et al. 2008).

Neutral particles associated with solar flares, such as γ -rays and neutrinos, are important to test theoretical aspects of particle acceleration in the magnetic reconnection because they can escape from the acceleration site¹. Their observation reveals both the spatial and time profile of primary particle acceleration while primary and secondary charged particles are trapped by the magnetic field.

¹ Some of line γ -rays cannot escape from the photosphere due to Compton scattering.

Neutrinos are only produced by accelerated protons above 300 MeV (Ramaty et al. 1975; Hudson & Ryan 1995), which can generate pions (π^\pm and π^0) by interacting with dense plasma in the lower solar atmosphere during solar flares. The generated π^\pm produce neutrinos in their decay chain. Figure 1 shows the typical neutrino fluxes from a powerful solar flare together with other neutrino fluxes, such as atmospheric neutrinos, solar neutrinos, and supernova relic neutrinos. In this article, we refer to such neutrinos from solar-flares as solar-flare neutrinos.

Solar-flare neutrinos have been searched for by neutrino detectors since the 1980s. However, no clear signal has been found in spite of setting a timing gate coincident with soft X-rays from visible solar flares. Setting a narrow search window, which covers only the period of neutrino production, de Wasseige (2016) and Okamoto et al. (2020) proposed to open search windows coincident with γ -rays originating from π^0 decays and nuclear interactions. These methods are helpful to minimize the background rate in the neutrino searches.

During the solar cycles 23 (1996–2008) and 24 (2008–2019), the Super-Kamiokande detector (hereafter SK) had been operating since April 1st, 1996 (Fukuda et al. 2003) with five distinct periods, from SK-I to SK-V with ultra-pure water. Although several neutrino telescopes are running during those solar cycles, SK is unique in its search for solar-flare neutrinos because its data set covers almost two cycles of solar activity. The largest solar flare, whose class is X28.0 and which occurred on November 4th 2003 (Kane et al. 2005), is also included.

This paper is organized as follows. In Section 2 we provide a brief overview of neutrinos associated with solar flares and the determination of the search windows to find solar-flare neutrinos. In Section 3 we describe the performance of the SK detector and the analysis methods to search for solar-flare neutrinos within the selected search windows. In Section 4 and Section 5 we present analysis results and make comparisons to results from other neutrino experiments. In the final section we conclude this study and give future prospects.

2. SOLAR-FLARE NEUTRINOS

2.1. Particle acceleration and neutrino production in solar flare

In many solar flares, the hard X-ray, (line) γ -ray, and microwave emissions are observed almost simultaneously (Chupp et al. 1981; Nakajima et al. 1983; Yoshimori 1984). Those observations suggest that electrons, protons, and ions are accelerated over a short period of time.

The γ -ray emissions from solar flares provide information on the processes of proton acceleration and the subsequent reactions of the protons in the chromosphere. For example, line γ -rays from neutron capture on hydrogen (Chupp et al. 1973) and de-excitation γ -rays from ^{12}C and ^{16}O (Smith et al. 2003) imply the acceleration and nuclear reactions of protons. The time profile of γ -rays from π^0 decays ($\pi^0 \rightarrow 2\gamma$) also provides information on the time scale of neutrino production since charged pions can be generated at the same time as neutral pions. Observations of γ -rays from π^0 decay have been performed by several instruments on-board satellites in geostationary and polar orbits (Forrest et al. 1986; Chupp et al. 1987; Leikov et al. 1993; Debrunner et al. 1997; Kanbach et al. 1993; Kurt et al. 2010; Ackermann et al. 2017). Those γ -ray observations indirectly demonstrate that protons are accelerated up to relativistic energies and subsequently neutrinos should be produced during solar flares.

On the theoretical side, several simulations of neutrino emission from solar flares have been developed in order to estimate the expected event rate in neutrino detectors. Table 1 summarizes the

Table 1. The summary of theoretical models for solar-flare neutrinos. In each theoretical model, the number of expected interactions in the SK detector are calculated. For the expected number of events in the SK detector from [Fargion & Moscato \(2003\)](#), the conversion factor (η defined in [Fargion & Moscato \(2003\)](#)) is assumed to be ~ 0.10 for the visible side and ~ 1.0 for the invisible side.

Theoretical model (Reference)	Side of the Sun	Power index of proton	Directional feature of generated neutrino	Number of expected events in SK [flare ⁻¹]
Kocharov et al. (1991)	Visible side	3–4	Isotropic	1.36×10^{-4}
Kocharov et al. (1991)	Invisible side	1	Beam like	0.85
Fargion (2004)	Visible side	–	Isotropic	0.75
Fargion (2004)	Invisible side	–	Beam like	7.5
Takeishi et al. (2013)	Invisible side	3	Isotropic	9.0×10^{-5}
Takeishi et al. (2013)	Invisible side	1	Beam like	3.8×10^{-6}

features of three theoretical models for solar-flare neutrinos by [Kocharov et al. \(1991\)](#), [Fargion & Moscato \(2003\)](#), and [Takeishi et al. \(2013\)](#).

These theoretical models describe neutrino emission from the most powerful solar flares whose energy is larger than 10^{31} erg. The neutrino fluxes change depending on the assumptions in the models, such as the proton spectral index, the interaction cross sections between accelerated protons and nuclei in the chromosphere, the angular distribution of neutrinos with respect to the proton direction, and the location of the solar flare as summarized in Table 1. Although the absolute fluxes are quite different, the predicted energy spectrum of solar-flare neutrinos is almost identical to the atmospheric neutrino energy spectrum. This is because in both cases neutrinos are created through the same production process.

[Fargion \(2004\)](#) estimated the number of neutrino interactions between neutrinos and the free protons in the water of the SK detector;

$$n_{\text{int}} = 7.5 \eta \left(\frac{E_{\text{FL}}}{10^{31} \text{ erg}} \right), \quad (1)$$

where n_{int} is the number of interactions in the SK detector (fiducial volume 22.5 kton), E_{FL} is the total energy of the solar flare, and η is an energy conversion factor from the solar flare E_{FL} to neutrino energy, as defined in [Fargion & Moscato \(2003\)](#). According to [Fargion \(2004\)](#), several neutrino interactions are expected in the SK detector when a solar flare classified as the largest explosion ($\geq 10^{32}$ erg) occurs on the visible (invisible) side of the Sun and $\eta \sim 0.10$ (1.0). On the other hand, [Takeishi et al. \(2013\)](#) argues that the assumed value of η is questionable and it is typically of order 10^{-6} . Therefore, experimental searches for neutrinos from powerful solar flares can test theoretical aspects of neutrino production during the impulsive phase of the solar flares.

2.2. Searches for solar-flare neutrinos using neutrino detectors

The possibility of detecting solar-flare neutrinos with neutrino experiments has been discussed since the 1980's ([Bazilevskaya et al. 1982](#); [Erofeeva et al. 1983](#)). In 1988, the Homestake experiment reported an excess of neutrino events when energetic solar flares occurred ([Davis 1994](#)). This observation suggested a possible correlation between solar flares and the neutrino capture rate on ^{37}Cl ([Bahcall 1988](#); [Bahcall et al. 1987](#)). Soon after the Mont Blanc Neutrino Detector searched for

solar-flare neutrinos but no significant signal was found in time coincidence with any solar flares that occurred between 1988 to 1991, including the largest solar flare in 1989 (Aglietta et al. 1991). Since then various neutrino detectors have searched for solar-flare neutrinos by analyzing different solar flare samples (Hirata et al. 1988, 1990; Gando et al. 2012; Aharmim et al. 2014; Agostini et al. 2021; Abbasi et al. 2021; Abe et al. 2022b). However, no significant signal for solar-flare neutrinos has been found by any of these experiments.

2.3. Search window for solar flares on the visible side of the Sun

Atmospheric neutrinos are continuously produced by collisions between primary cosmic rays and nuclei in the Earth’s atmosphere (Richard et al. 2016). In neutrino experiments the separation between atmospheric neutrinos and solar-flare neutrinos is technically difficult since their energy ranges overlap with each other due to their identical production process. While atmospheric neutrinos are generated constantly, solar-flare neutrinos are released only during the period of particle acceleration during the flare. Therefore, a search window that is appropriately narrow in time allows neutrino detectors to substantially reduce the atmospheric neutrino background rate.

The first proposal to use search windows when searching for solar-flare neutrinos was published by de Wasseige (2016), which analyzed the detection time of γ -rays from π^0 decays using the Fermi-Large Area Telescope (LAT) satellite (Atwood et al. 2009). Following this proposal, the IceCube collaboration searched for neutrinos from solar flares in the energy range from 500 MeV to 5 GeV (Abbasi et al. 2021) and constrained the integrated neutrino flux emitted during the considered time window according to the catalog of γ -ray flares recorded by Fermi-LAT (Ajello et al. 2021). However, this catalog covers the period of solar cycle 24 (2008–2019) after the launch of Fermi-LAT in 2008. Hence, a different method must be used to identify search windows for solar flares that occurred before 2008.

Okamoto et al. (2020) proposed to determine the search window by analyzing 2.2 MeV line γ -rays and the derivative of soft X-rays to improve the signal-to-noise ratio to find solar-flare neutrinos. The former channel selected three solar flares across solar cycles 23 and 24 with the observation of line γ -rays recorded by the RHESSI satellite² (Lin et al. 2002) on July 23rd 2002 (X5.1), November 2nd 2003 (X9.2), and January 20th 2005 (X7.1). The latter channel selected twenty-three solar flares (above X5.0) recorded by the GOES³ (Lemen et al. 2004) across solar cycles 23 and 24. Note that this selection set the search window for the largest flare (X28.0) on November 4th, 2003. Although the derivative of soft X-rays extracts the time scale of non-thermal electron acceleration in general, this channel is still appropriate to improve the signal-to-noise ratio for finding solar-flare neutrinos because the recent study by Fermi-LAT concluded ions and electrons are accelerated, transported, and interact with the ambient medium at the same time (Ajello et al. 2021). In the latter section, we separately searched in the SK detector for neutrinos from selected solar flares occurred on the visible side of the Sun within these two different search windows.

2.4. Search windows for solar flares on the invisible side of the Sun

Energetic proton flux directed back to the Sun generates a nuclear cascade in the solar atmosphere. Such flux results in narrow beam of relativistic protons with a rather hard spectrum from solar flares on the invisible side of the Sun. Hence the searches for neutrinos associated from solar flares

² The Reuven Ramaty High-Energy Solar Spectroscopic Imager (RHESSI)

³ Geostationary Operational Environmental Satellite (GOES)

occurring at the invisible side provide information about acceleration mechanism of downward going proton flux. [Fargion & Moscato \(2003\)](#) argue that the probability of solar-flare neutrino detection increases when solar flares occur on the invisible side of the Sun due to efficient collisions between the accelerated protons and the dense plasma at the surface of the Sun. Searching for neutrinos from solar flares on the invisible side of the Sun allows us to test these proposed neutrino production models. However, a selection of solar flares that occur on the invisible side of the Sun has never been performed for this purpose.

To select solar flares that occur on the invisible side of the Sun, the time of CME emission allows one to infer the occurrence time of solar flares because large energetic solar flares are usually accompanied by CMEs ([Andrews 2003](#)). The observation of CMEs occurring on the invisible side of the Sun has been performed by the LASCO⁴ coronagraph ([Domingo et al. 1995](#); [Brueckner et al. 1995](#)) and the CME emission times are listed in a catalog maintained by NASA ([Yashiro et al. 2004](#)).

From the catalog we selected energetic CMEs whose emission speed is more than 2000 km s^{-1} , which roughly corresponds to class X2.0 solar flares. This criteria allowed us to select ten CMEs from 1996 April to 2018 May. The search window for solar flares occurring on the invisible side is set to 7238 s as explained in Appendix A. The date of the selected CMEs is summarized in Table 9 in Appendix A.

3. DETECTOR AND ANALYSIS

3.1. *The Super-Kamiokande detector*

Super-Kamiokande is a water Cherenkov detector in a cavern beneath Ikeno-yama mountain, Japan ([Fukuda et al. 2003](#)). It is a cylindrical stainless tank structure and contains 50 kiloton (ktons) of ultra-pure water. The detector is divided into two regions by the tank structure, separated optically by Tyvek sheets: one is the inner detector (ID) and the other is the outer detector (OD). The ID serves as the target volume for neutrino interactions and the OD is used to veto external cosmic-ray muons as well as γ -rays from the surrounding rock. In the ID, the diameter (height) of the cylindrical tank is 33.8 m (36.2 m). It contains 32 kton of water and holds 11,129 inward-facing 20-inch photomultipliers (PMTs)⁵ to observe the Cherenkov light produced by charged particles. The diameter (height) of the OD tank is 39.3 m (41.4 m). The detector simulation has been developed using the GEANT3 toolkit ([Brun et al. 1994](#)) and tuned to calibration data. The details of the detector configuration, the calibration, and the performance can be found elsewhere ([Abe et al. 2014](#)). In this article, we analyzed the data taken in SK-I through SK-IV (from April 1996 to May 2018) to cover solar cycles 23 and 24⁶.

In order to determine the initial neutrino interaction vertex and the trajectories and momenta of any subsequent charged particles, event reconstruction is performed by analyzing the timing and the ring pattern of the observed Cherenkov light in the SK detector. Using this water Cherenkov technique the SK detector has sensitivity to a wide range of neutrino energies, from a few MeV to tens of GeV. The neutrino events are categorized into two samples depending on the energy of the reconstructed charged particles after the initial neutrino interaction. A neutrino event reconstructed with less than 100 MeV of visible energy is categorized as part of the “low energy sample” and is mainly used for studies of solar neutrinos ([Abe et al. 2016](#)) and supernova neutrinos ([Abe et al.](#)

⁴ The Large Angle Spectroscopic Coronagraph (LASCO) on the Solar and Heliospheric Observatory (SOHO)

⁵ The SK-I detector used 11,149 PMTs while the other phases use 11,129 PMTs except for SK-II, which used 5,182.

⁶ During SK-V (from January 2019 to July 2020), no solar flare above X5.0 occurred due to low solar activity.

2021). In this energy region the reconstruction tool searches for an interaction point because the track length of the charged particle is at most 30 cm, which is small compared to the reconstructed vertex resolution (typically more than 50 cm). On the other hand, a neutrino event reconstructed with more than 100 MeV of visible energy is categorized as part of the “high energy sample” and is mainly used for the study of atmospheric neutrinos (Richard et al. 2016) and to search for proton decay (Takenaka et al. 2020). In this energy region the majority of neutrino interactions occur on nuclei and can produce a number of charged particles. The event reconstruction algorithm then determines the number of Cherenkov rings in the event, identifies the particle type that created each ring, locates the interaction vertex and predicts the energy of each charged particle.

3.2. Low energy sample

The SK detector can potentially reconstruct the energies of charged particles down to a few MeV. In the energy range of the low energy sample, the dominant reaction is the inverse beta decay (IBD) of electron anti-neutrinos because of its relatively large cross section. Other sub-dominant reactions are elastic scattering between electrons and electron neutrinos, and the charged current and neutral current interactions with oxygen (Kolbe et al. 2002). Even though we set an appropriate search window for solar-flare neutrinos, the signal-to-noise ratio is still poor below 16 MeV due to solar neutrinos and background events originated from radioactive isotopes dissolved in the SK water (Nakano et al. 2020) and produced by penetrating muons (Zhang et al. 2016). Hence, we set the energy threshold to 16 MeV in this analysis, where the total energy of a positron produced by the IBD is considered. For the energy range above 16 MeV, the possible backgrounds are atmospheric neutrino interactions, decay electrons originated from invisible muons, and low energy pions. For selecting positrons from IBD reactions we applied the selection cuts used for supernova relic neutrino searches since these cut criteria are optimized to maximize the event selection efficiency of the positron. The detailed analysis method is described in Bays et al. (2012) and Abe et al. (2021).

For evaluating the event selection efficiency in the low energy sample, we first simulated positrons from IBD reactions. In this simulation, we use the neutrino energy spectrum from Fargion & Moscato (2003). Then, the positron energy is calculated by considering the cross section of the IBD reaction from Strumia & Vissani (2003). Note that only the IBD reaction is considered in this simulation because of its large cross section in this energy range. Figure 2 (left-top) shows the input energy distribution of positrons from the neutrino interactions and the reconstructed total positron energy after selection cuts.

Assuming the electron anti-neutrino energy spectrum of Fargion & Moscato (2003), the selection efficiency, defined as $\varepsilon_{\text{low}}^{\text{Fargion}}$, in the low energy sample is about 27%, since the energy range covered by the low energy sample is relatively narrow. We also evaluated the selection efficiency for neutrinos between 16 and 100 MeV by generating a flat neutrino energy distribution. This produced the model independent analysis detailed in Section 5.2. That selection efficiency, defined as $\varepsilon_{\text{low}}^{\text{Ind}}$, is about 75%. Table 2 summarizes the livetime, the selection efficiencies, and the background rate after all reduction cuts in the low energy sample using all of the SK data sets.

After the installation of new front-end electronics at SK-IV (Yamada et al. 2010), the SK trigger system allows the detector to tag neutron signals after IBD reactions using the delayed coincidence technique. However, we did not require the neutron signal to identify electron anti-neutrinos in this analysis since the trigger system did not allow us to record the neutron signals in SK-I, -II, and -III.

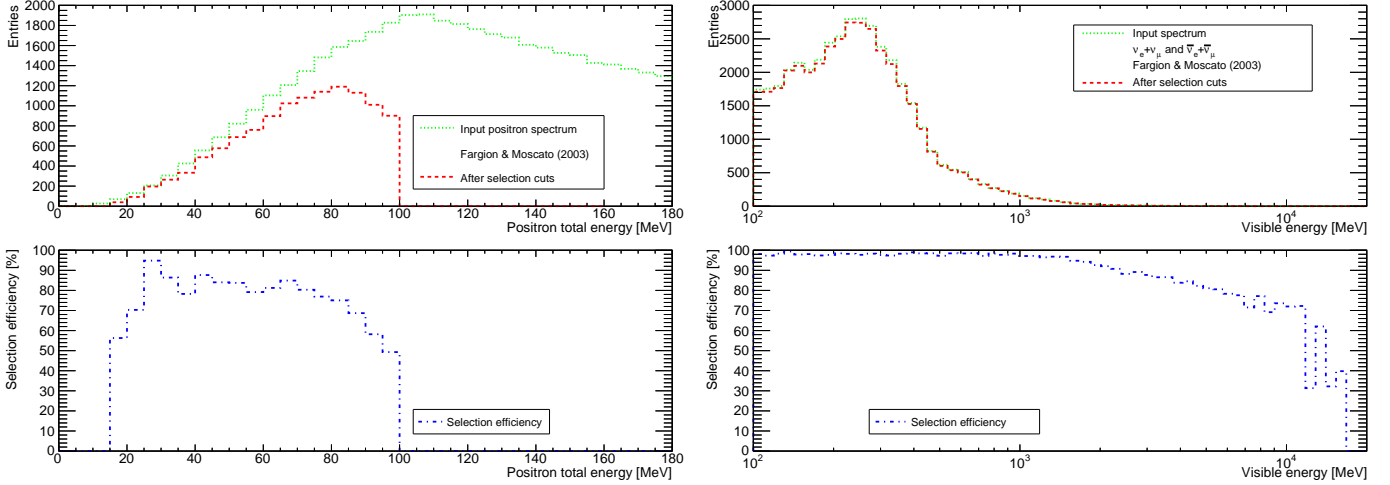


Figure 2. Energy spectra and selection efficiencies for the low (left) and high (right) energy samples. The distributions of the reconstructed positron energy and the visible energy calculated using the MC simulation which uses the energy spectra of solar-flare neutrinos from [Fargion & Moscato \(2003\)](#). The horizontal axis is reconstructed positron kinetic energy in the left panel (reconstructed visible energy in the right panel), and the vertical axis shows the number of events. The light-green histograms represent the energy spectra of the generated events and the red histograms represent the energy spectrum after the selection cuts are applied. The blue histograms represent the selection efficiencies.

Table 2. The summary of the dates, the livetimes, the selection efficiencies ($\epsilon_{\text{low}}^{\text{Fargion}}$ and $\epsilon_{\text{high}}^{\text{Fargion}}$) for the energy spectrum from [Fargion & Moscato \(2003\)](#), the model-independent selection efficiencies ($\epsilon_{\text{low}}^{\text{Ind}}$), and the background rates of the low energy sample and the high energy sample. The difference in their livetimes comes from differences in the SK detector data quality between the low and high energy analyses.

Category	SK phase	SK-I	SK-II	SK-III	SK-IV
Date	Start	Apr. 1996	Oct. 2002	Jul. 2006	Sep. 2008
	End	Jul. 2001	Oct. 2005	Aug. 2008	May 2018
Low energy	Livetime [day]	1497	794	562	2970
	Selection efficiency ($\epsilon_{\text{low}}^{\text{Fargion}}$) [%]	26.2	27.1	27.8	28.3
	Selection efficiency ($\epsilon_{\text{low}}^{\text{Ind}}$) [%]	72.3	74.8	76.6	78.1
	Background rate [event day ⁻¹]	0.20 ± 0.01	0.19 ± 0.02	0.20 ± 0.01	0.19 ± 0.01
High energy	Livetime [day]	1489	825	522	3235
	Selection efficiency ($\epsilon_{\text{high}}^{\text{Fargion}}$) [%]	61.9	62.1	61.8	61.6
	Background rate [event day ⁻¹]	7.45 ± 0.07	7.33 ± 0.09	7.53 ± 0.12	7.48 ± 0.05

3.3. High energy sample

This sample is further divided into three sub-samples based on the event topology: a fully contained (FC) sample, a partially contained (PC) sample, and an upward going muon (UPMU) sample. In this study, we only analyzed the FC sample because the energy of solar-flare neutrinos is less than 10 GeV and this results in the tracks of the all charged particles being essentially contained in the

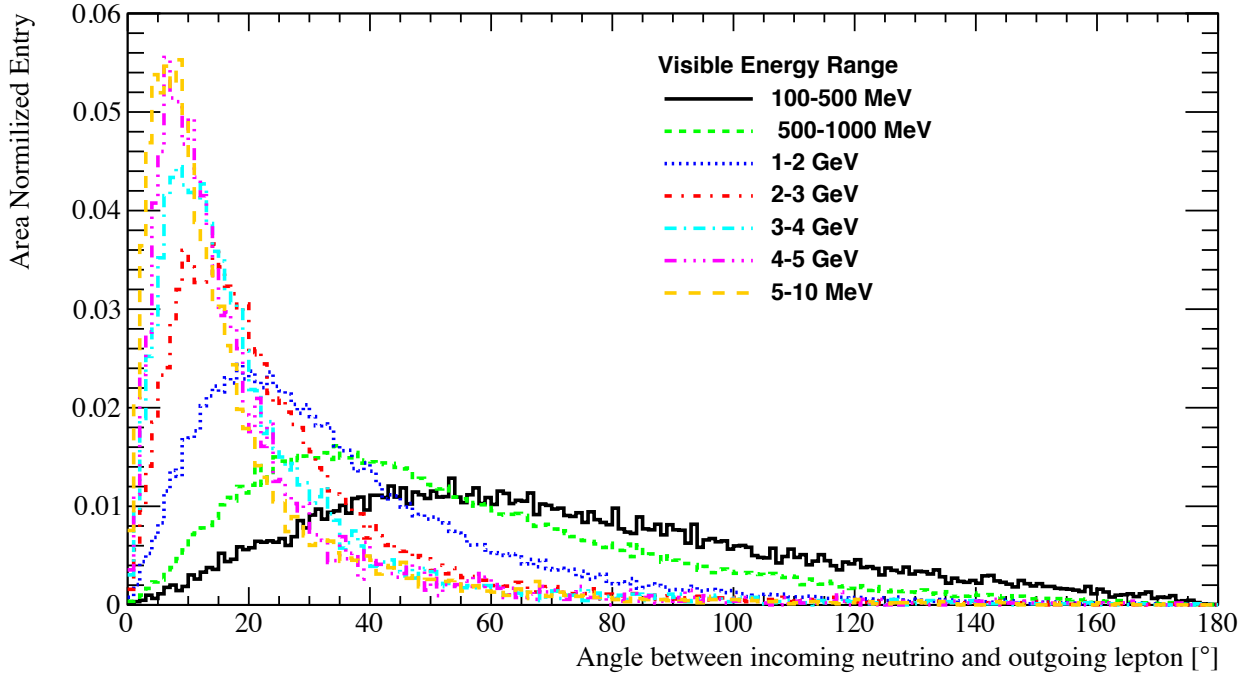


Figure 3. Angular distribution between the direction of the incident neutrino and the reconstructed directions of produced charged particles (e^\pm , μ^\pm , and π^\pm) from the MC simulation of the high energy sample. For multi-ring events, the direction of the neutrino is reconstructed as the momentum weighted sum of the directions of all the identified rings.

inner tank. In the energy region of the high energy sample different interactions occur depending on the neutrino energy. For simulating neutrino interactions with hydrogen and oxygen in the detector, we used the NEUT generator (Hayato & Pickering 2021). Figure 2 (right-top) shows the input energy distribution of charged particles from the neutrino interactions and the reconstructed energies after selection cuts. The event selection criteria for the high energy sample are detailed in Ashie et al. (2005). The selection efficiency for the neutrino spectrum from Fargion & Moscato (2003) is typically 62% after all reduction cuts. Table 2 also summarizes the livetime, the selection efficiency, and the background rate of the high energy sample for each SK phase.

Directional information can be used to test whether neutrino signals come from a specific astrophysical source or not. Figure 3 shows the typical distribution of angles between the incoming neutrino and the direction of the final state charged particles based on the MC simulation. In the energy region above 1 GeV the direction of the final state charged particles is highly correlated with the direction of the incoming neutrino and this tendency clearly depends on the neutrino energy.

4. RESULTS

4.1. Results for solar-flare neutrinos coincident with line γ -ray observations

As explained in Section 2.1, 2.2 MeV line γ -rays are produced by the acceleration of hadrons, their interactions with nuclei in the chromosphere, and the production of neutrinos. Hence, the signal-to-noise ratio of solar-flare neutrinos is high when in coincidence with line γ -rays. For this reason, we searched for neutrino candidate events within the search windows determined by the light curve of

Table 3. Summary of two events observed within the search window for neutrinos associated with a solar flare on the visible side of the Sun. The estimated background rate is normalized by the duration of the corresponding search window determined by Okamoto et al. (2020).

Date (UTC)	November 4th, 2003	September 6th, 2017
Solar flare class	X28.0	X9.4
SK phase	SK-II	SK-IV
Observed time (UTC)	19:42:26	12:03:05
Duration of window [s]	1144	521
Event topology	2-ring e -like	1-ring μ -like
Reconstructed energy	178.3 MeV	1.2 GeV
θ_{Sun}	67.1°	39.6°
Estimated background rate [event flare ⁻¹]	0.20	0.12
p -value of the null hypothesis	18.1%	11.3%

line γ -rays by Okamoto et al. (2020). As explained in Section 2.3, three solar flares on the visible side of the Sun are selected by Okamoto et al. (2020). The SK data does not cover the period of the solar flare that occurred on July 23rd 2002 due to the re-instrumentation of the SK detector following the implosion accident in 2001. Within the remaining two search windows no signal was found in either the low or high energy samples.

4.2. Results for solar flares on the visible side of the Sun

We searched for solar-flare neutrinos from the visible side of the Sun within the search windows determined by the time derivative of soft X-rays recorded by the GOES satellite, as described in Section 2.3. Okamoto et al. (2020) selected twenty-three solar flares using this channel, with SK missing three of these (on August 25th 2001, December 13th 2001 and July 23rd 2002) because of the re-instrumentation work discussed previously. Hence, we searched for neutrinos from twenty solar flares across solar cycles 23 and 24. No signal was found in the low energy sample while two events are found in the high energy sample. The first event was observed on November 4th 2003 and the second event on September 6th 2017, as summarized in Table 3.

Figure 4 shows the time of the observed neutrino events together with the light curves recorded by the GOES satellite. The event on November 4th 2003 was observed during the impulsive phase of the solar flare, where particle acceleration is expected to be active. Furthermore, Watanabe et al. (2006) reported that relativistic neutrons associated with this solar flare were observed by the neutron monitors on the ground at 19:45 (UTC), which is about 3 minutes after the detection of the neutrino candidate in SK. This simultaneous observation also indicates that hadrons (ions) were accelerated to more than 1 GeV during this solar flare. On the other hand, the event on September 6th 2017 was observed during the dimming phase after the peak of the soft X-ray light curve, when all processes of particle acceleration are likely to have been completed. The event displays and sky-maps for the two observed candidates are shown in Figure 13 and Figure 14 in Appendix B.

Figure 5 shows the energies of the two observed events compared to the expected background energy spectrum. Here, the background spectrum is from events accumulated outside the search windows and the main component is the interaction of atmospheric neutrinos. The expected number

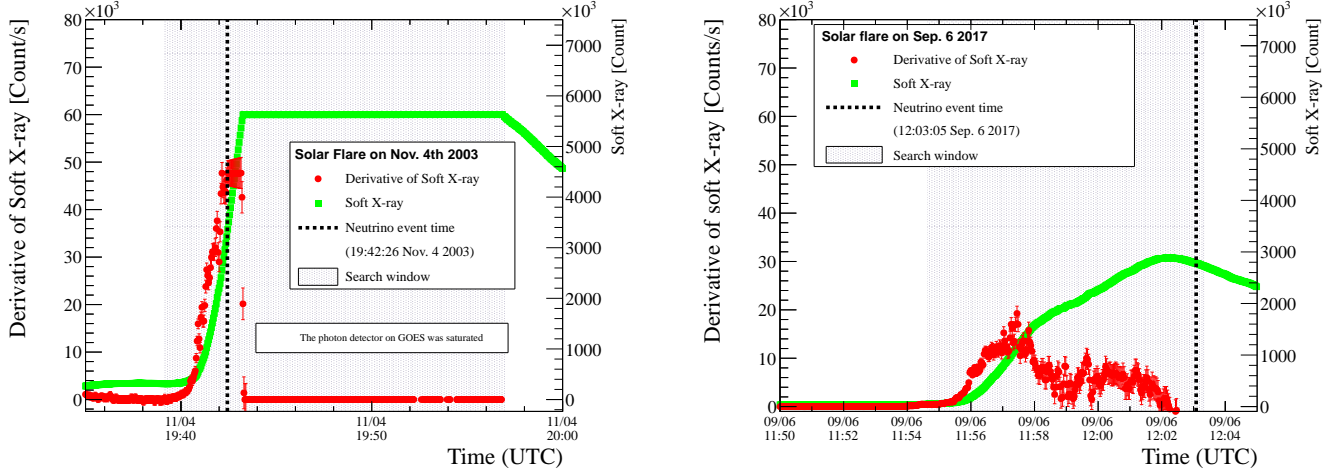


Figure 4. The time of observed neutrino events for the solar flare on November 4th, 2003 (left), and July 6th, 2017 (right). The black vertical line shows the time of neutrino event in the SK detector. The red (green) plot shows the derivative of the light curves (original light curve) recorded by the GOES satellite. The shaded region shows the search windows determined by using the derivative of soft X-ray according to the method developed by Okamoto et al. (2020). In the case of the solar flare on November 4th, 2003 (left), the instrument on the GOES satellite saturated due to the high intensity of soft X-rays. That resulted in the satellite not recording data for more than 15 minutes from 19:45 to 20:00.

of background events in the high energy sample in the search window is 0.20 events (0.12 events) for the solar flare event on November 4th 2003 (September 6th 2017). The p -value of the null hypothesis is 18.1% (11.3%).

In order to investigate whether neutrino candidate events come from the direction of the Sun or not, we examined the angular distribution of θ_{Sun} , which is defined as the angle between the reconstructed direction of the charged particles and the direction pointing to the Sun. In the case of a multi-ring event, the direction of the neutrino is reconstructed as the momentum weighted sum of the directions of all the identified rings. The value of θ_{Sun} of the candidate event on November 4th, 2003 (September 6th, 2017) is 67.1° (39.6°). Figure 6 shows the θ_{Sun} of the two observed events together with the angular distribution derived from the MC simulation.

4.3. Results for solar flares on the invisible side of the Sun

As explained in Section 2.4, we selected ten large CMEs that occurred on the invisible side of the Sun by setting criteria on their emission speed. However, SK did not take data for the two CMEs that occurred on July 18th and 19th, 2002 due to the detector re-instrumentation work. Hence, we searched for solar-flare neutrinos from the remaining eight CMEs that occurred on the invisible side of the Sun.

There was no signal in the low-energy sample while six events were found in the high-energy sample as summarized in Table 4. Two neutrino events were identified for the solar flares on November 7th, 2003 and July 24th, 2005 while one event was observed for those on June 4th, 2011 and July 23rd, 2012. The expected number of background events in the high-energy sample is 0.62 event flare⁻¹. The p -value for the null hypothesis finding one (two) events for these solar flares is 10.2% (33.5%). Figure 7 shows the energies of the observed events together with the background energy spectrum. The event displays and sky-maps for the two observed candidates are shown from Figure 15 to

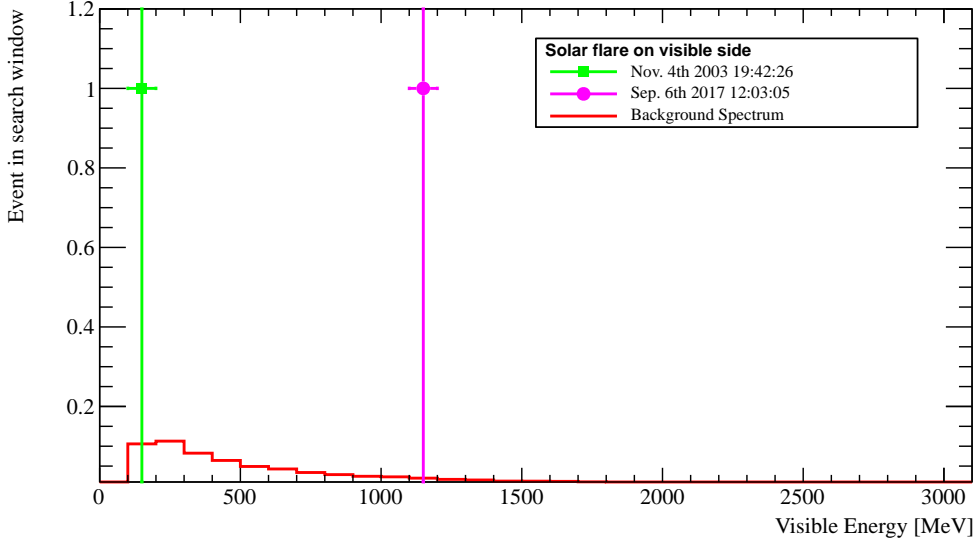


Figure 5. The energy distribution of the simulated neutrino events from solar flares occurring on the visible side of the Sun compared to the background sample. The first event (in the green square) was observed as a 2-ring e -like event on November 4th, 2003 while the other (in the magenta circle) was observed as a 1-ring μ -like event on September 6th, 2017. The background spectrum (red histogram) is normalized such that it corresponds to the expectation for a search window with an average duration of 700 s, determined from the derivative of the soft X-ray light curve by Okamoto et al. (2020).

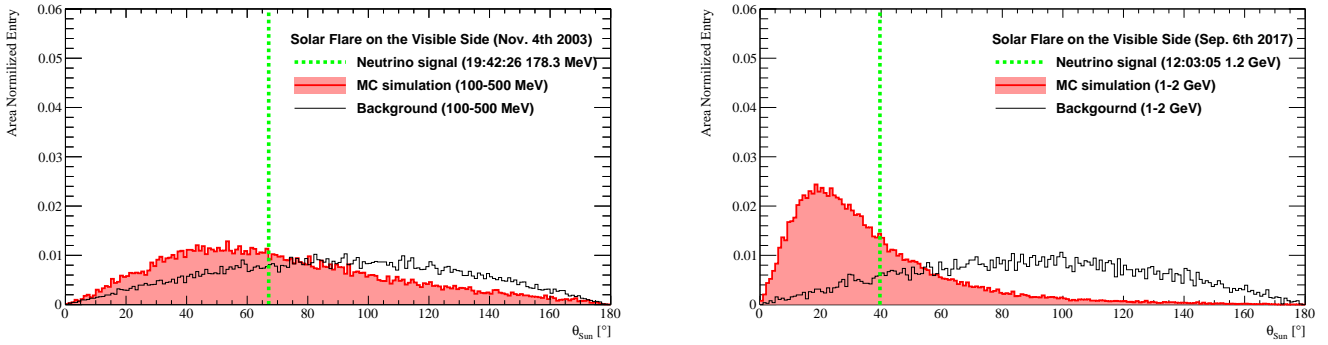


Figure 6. Reconstructed angles of the observed neutrino events in coincidence with solar flares occurring on November 4th, 2003 (left panel) and September 6th, 2017 (right panel) together with the angular distributions from MC sample for signal and background. The light green dashed line shows the angles between the reconstructed event direction and the direction of the Sun, θ_{Sun} , at the time when the neutrino event was observed. The red (black) histograms show the angular distribution of the MC (background) sample in the given energy range.

Figure 18 in Appendix C.

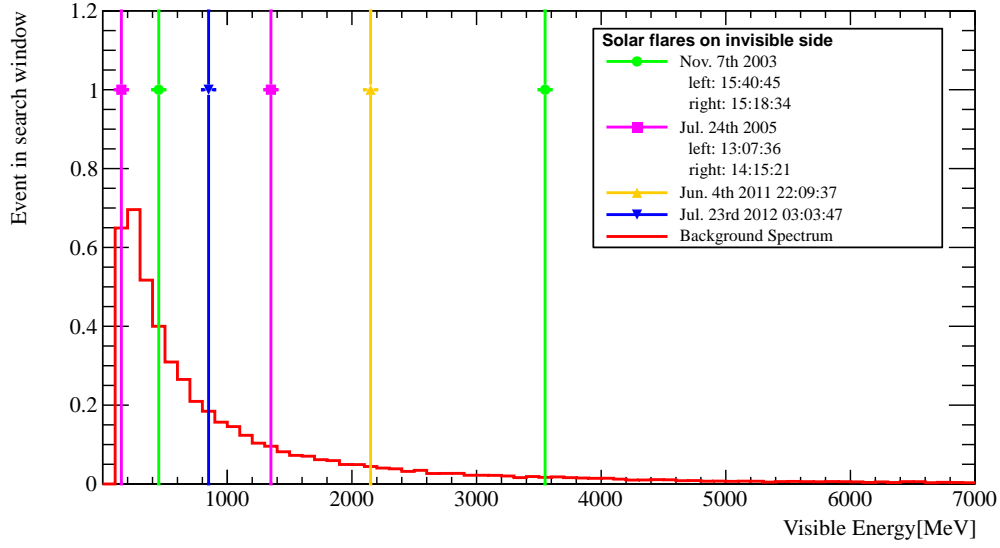


Figure 7. The reconstructed energies of the neutrino events from solar flares that occurred on the invisible side of the Sun and the typical energy distribution of events in the background sample. The green circles, magenta squares, yellow upward triangles, and blue downward triangles are the energy of observed events on November 7th, 2003, July 24th, 2005, June 4th, 2011, and July 23rd, 2012, respectively. The background spectrum is normalized by the time duration of 7238 s according to the method described in Appendix A.

Table 4. The summary of events observed within the search window for neutrinos associated with solar flares that occurred on the invisible side of the Sun. The duration of the search window is 7238 s as detailed in Appendix A. The number of expected background events in the search window is 0.62 ± 0.01 .

Date (UTC)	November 7th, 2003	July 24th, 2005	June 4th, 2011	July 23rd, 2012
SK phase	SK-II	SK-II	SK-IV	SK-IV
Observed time (UTC)	15:18:34	13:07:36	21:05:07	03:03:47
Time difference between two events	1131 s	4065 s	–	–
Event topology	1-ring e -like	1-ring μ -like	4-ring e -like	3-ring two μ -like, e -like
Reconstructed energy	3.58 GeV	126 MeV	2.14 GeV	834 MeV
θ_{Sun}	20.0°	100.4°	101.0°	76.7°
p -value of the null hypothesis	10.2%	10.2%	33.5%	33.5%
Probability of background event from timing distribution	10.2%	34.5%	–	–

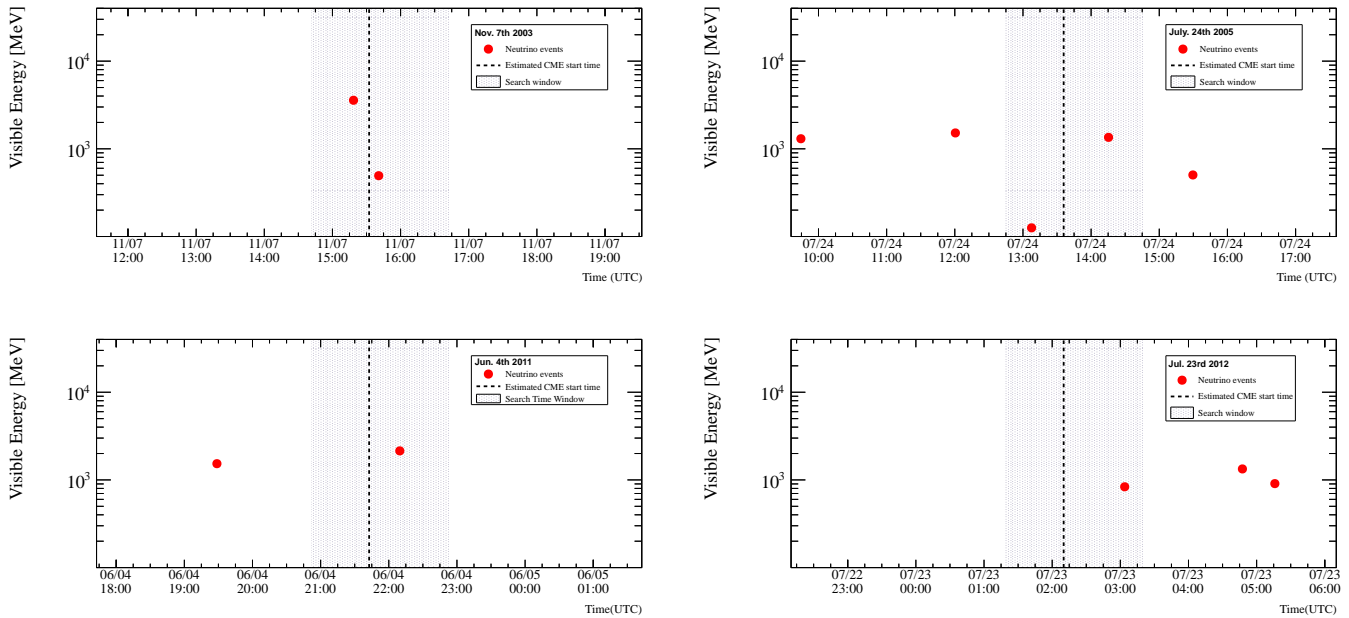


Figure 8. The time distributions of neutrino events around the solar flares that occurred on the invisible side of the Sun on November 7th, 2003 (top-left), July 24th, 2005 (top-right), June 4th, 2011 (bottom-left), and July 23rd, 2012 (bottom-right). The red points show the times of the neutrino events, which are summarized in Table 4. The dashed vertical lines show the estimated start time of the particular CME emission and the shaded regions show the search windows (7238 s) according to the method described in Section 2.4.

Figure 8 shows the observed neutrino events around the time of the solar flare. Note that the duration of the search window for solar flares on the invisible side of the Sun is uniform (7238 s) as detailed in Appendix A.

In the case of the two solar flares on November 7th, 2003 and on July 24th, 2005, we found two consecutive neutrino events within their search windows. Their time differences are 1131 s and 4065 s, respectively. We analyzed the time difference distribution between consecutive events in the background sample in order to verify whether their time differences are likely or not. Figure 9 shows the time difference of the two consecutive events observed within their search windows together with the time difference distribution of the background sample. Comparing the time difference distribution of the background sample, we estimated the occurrence probabilities for each solar flare, which correspond to 10.2% and 34.5%, respectively.

Figure 10 shows the reconstructed angle θ_{Sun} together with the typical distribution derived from the MC simulation. The reconstructed values of θ_{Sun} are also summarized in Table 4.

5. DISCUSSION

5.1. solar-flare neutrino fluence derived from the theoretical predictions

We estimated the fluence of solar-flare neutrinos produced by powerful solar flares based on the number of observed events within their corresponding search window. Here, we calculate the upper limit of the neutrino fluence using a Bayesian method, in the absence of a significant excess of observed

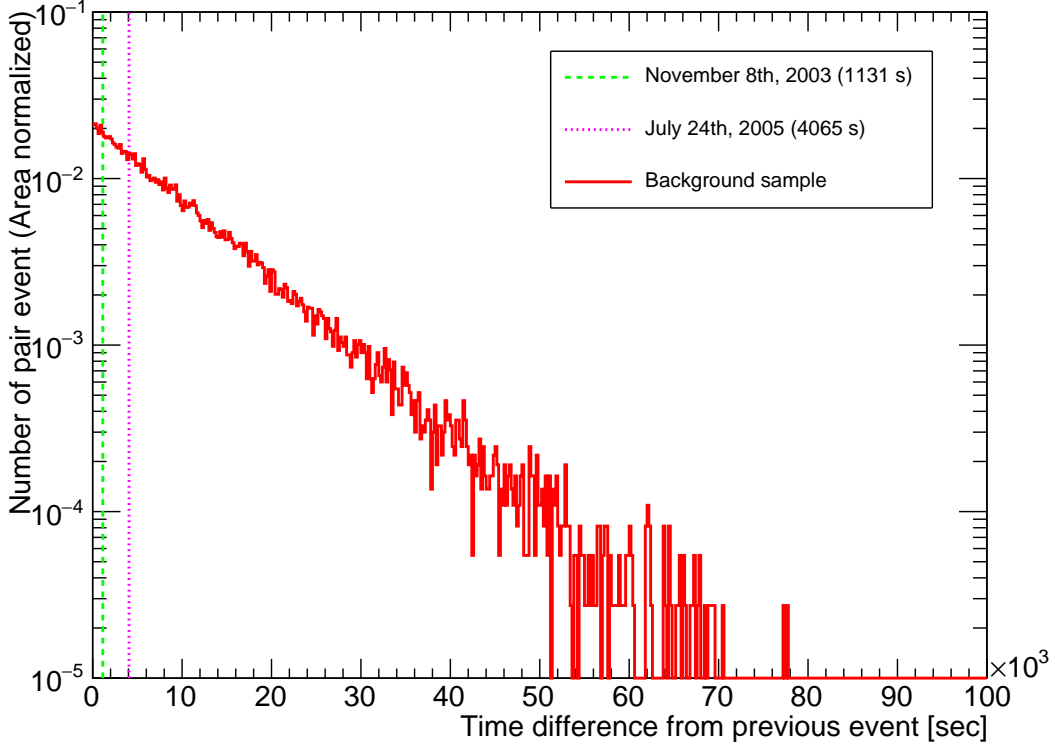


Figure 9. The time difference between the two events observed within the search windows for solar flares on November 7th, 2003 (1131 s, dashed green line) and July 24th, 2005 (4065 s, dotted pink line). The red histogram shows the distribution of the time difference between consecutive events in the background sample using the combined data from SK-I to SK-IV.

events above the expected background rate (Roe & Woodroffe 2000). We separately calculate the upper limits of neutrino fluence for low and high energy samples depending on the neutrino energies.

The neutrino fluence at the Earth Φ is calculated using the neutrino flux $F(E_\nu)$ at the Earth in the search window,

$$\Phi = t_{\text{emit}} \int F(E_\nu) dE_\nu, \quad (2)$$

where t_{emit} is a time duration of neutrino emissions in a solar flare, which is 100 s according to the assumption in Fargion & Moscato (2003), E_ν is the neutrino energy, and $F(E_\nu)$ is the predicted neutrino flux without neutrino oscillations in unit of $\text{cm}^{-2} \text{s}^{-1} \text{MeV}^{-1}$. We note that the duration of the search windows is sufficient to cover the duration of neutrino emission t_{emit} .

For the low energy sample, the expected number of neutrino interactions within the search window S is calculated using the following equation:

$$S \equiv N_p t_{\text{emit}} \int [F(E_{\bar{\nu}_e}) P_{ee} + F(E_{\bar{\nu}_\mu}) P_{\mu e}] \sigma_{\text{IBD}}(E_{\bar{\nu}_e}) \varepsilon_{\text{low}}^{\text{Fargion}}(E_{\bar{\nu}_e}) dE_{\bar{\nu}_e}, \quad (3)$$

where N_p is the number of target protons in the SK fiducial volume relevant to the neutrino interactions, $P_{\alpha\beta}$ is the probability for a neutrino produced as flavor α to oscillate to flavor β when travelling from the Sun to the Earth, σ_{IBD} is the IBD cross section as a function of electron anti-neutrino energy

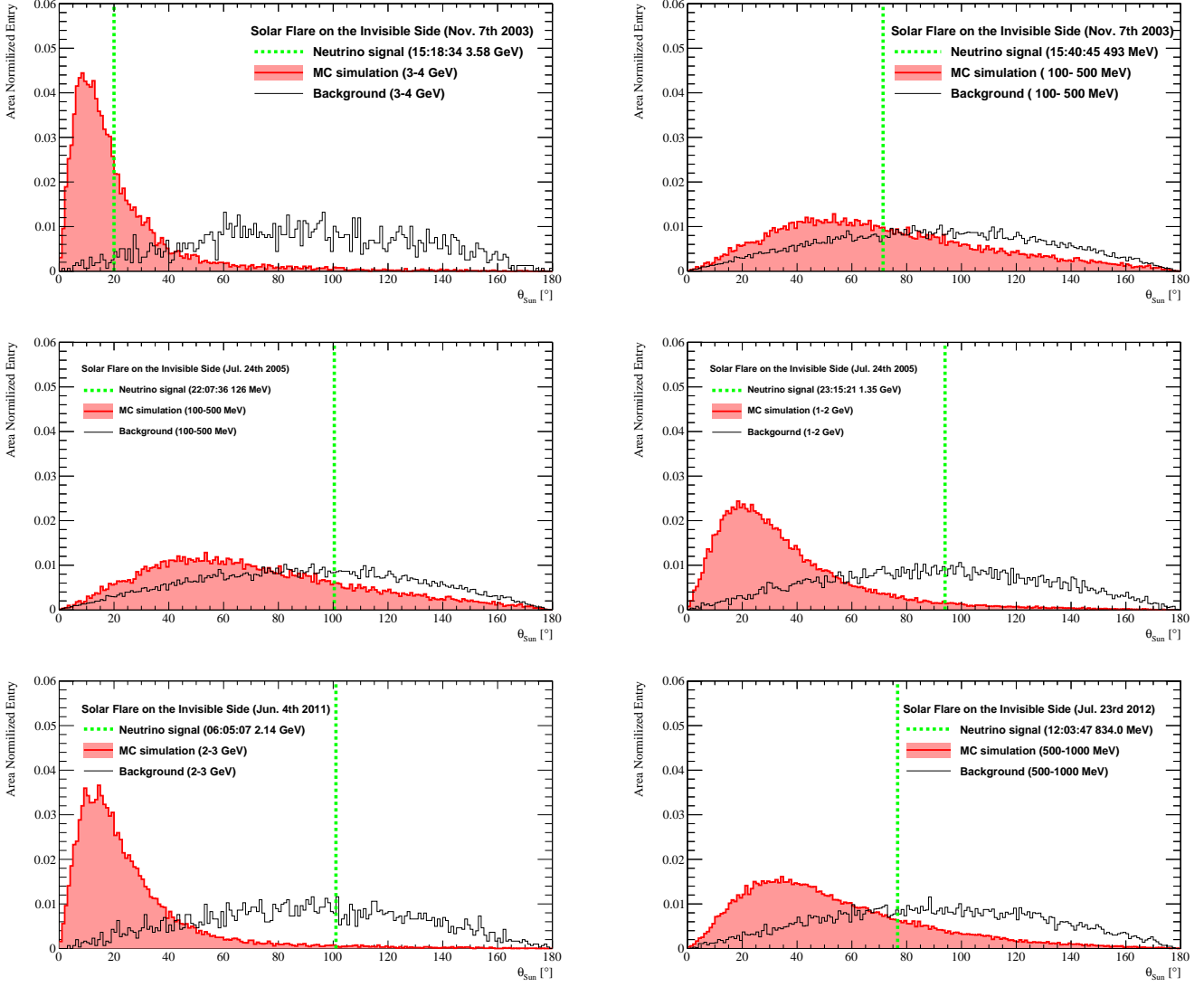


Figure 10. The reconstructed angle of the neutrino events in coincidence with solar flares that occurred on the invisible side of the Sun together with the typical angular distributions from the MC simulation for signal and background sample. The light green dashed lines show the angle between the reconstructed event direction and the direction from the Sun to SK, θ_{Sun} , at the time when the neutrino candidate was observed. The red (black) histograms show the angular distributions of the MC (background) sample in the given energy range.

derived from the theoretical model from [Strumia & Vissani \(2003\)](#) and $\varepsilon_{\text{low}}^{\text{Fargion}}$ is the event selection efficiency of the low energy sample defined in Section 3.

Using this expected number of neutrino interactions within the search window, the probability density function for the number of observed events is defined as follows:

$$P_{\text{low}}(S + B | n_{\text{obs}}) = \frac{1}{A} \iiint \frac{e^{-(S+B)} (S + B)^{n_{\text{obs}}}}{n_{\text{obs}}!} P(\sigma_{\text{IBD}}) P\left(\varepsilon_{\text{low}}^{\text{Fargion}}\right) P(B) d\sigma_{\text{IBD}} d\varepsilon_{\text{low}}^{\text{Fargion}} dB, \quad (4)$$

Table 5. A summary of systematic uncertainties in this analysis. The systematic uncertainties for the event selection efficiency of the low and high energy samples are estimated from Abe et al. (2021) and Abe et al. (2018a), respectively. The systematic uncertainty of the neutrino cross section for the low energy sample simulations has been taken from Strumia & Vissani (2003). For the high energy sample, the difference between the cross sections from Smith & Moniz (1972) and from Nieves et al. (2004) is assigned as the systematic uncertainty of the cross section. The deviation of the background rate which is listed in Table 2 has been used as the systematic uncertainty of the background rate.

Valuable	Low energy sample				High energy sample			
	SK-I	SK-II	SK-III	SK-IV	SK-I	SK-II	SK-III	SK-IV
Selection efficiency (δ_ε)	5.0%	5.3%	3.5%	4.1%	1.5%	0.4%	1.5%	0.1%
Cross section (δ_σ)	1.0%				20.0%			
Background rate (δ_B)	5.0%	10.5%	5.0%	5.3%	0.9%	1.2%	1.6%	0.6%

where B is the number of expected background events in the search window, A is a normalization factor representing the total integral of $P(S + B|n_{\text{obs}})$, and n_{obs} is the number of observed events in the search window. To include the effect of systematic uncertainties, $P(\sigma_{\text{IBD}})$, $P(\varepsilon_{\text{low}}^{\text{Fargion}})$, and $P(B)$ are introduced as the prior probabilities for fluctuations of the IBD cross section, the event selection efficiency, and the number of expected background events in the search window, respectively. The priors are assumed to follow a Gaussian distribution,

$$G(x) = \frac{1}{\sqrt{2\pi\delta_x^2}} \exp\left[-\frac{(x - x_0)^2}{2\delta_x^2}\right], \quad (5)$$

where x stands for the parameters σ_{IBD} , ε_{low} , and B , respectively, x_0 is their best estimates, and δ_x stands for their systematic uncertainties, expressed as $\delta_{\sigma_{\text{IBD}}}$, $\delta_{\varepsilon_{\text{low}}}$, and δ_B , respectively. For the systematic uncertainty of the IBD cross section (σ_{IBD}), we assigned the uncertainty estimated in Strumia & Vissani (2003). For the systematic uncertainty of the selection efficiency ($\delta_{\varepsilon_{\text{low}}}$), the variation in the number of events after all reduction cuts was evaluated by artificially changing the reduction parameters as performed in Abe et al. (2021). For the systematic uncertainty of the background rate (δ_B), the deviation of the actual background rate is conservatively assigned. Table 5 summarises the values of these systematic uncertainties.

With these definitions, the neutrino fluence at a given confidence level (C.L.) is calculated as

$$\text{C.L.} = \frac{\int_0^{\Phi_{\text{limit}}} P_{\text{low}}(S + B|n_{\text{obs}})d\Phi}{\int_0^\infty P_{\text{low}}(S + B|n_{\text{obs}})d\Phi}, \quad (6)$$

where Φ_{limit} is the upper limit of the neutrino fluence to be obtained.

Table 6 summarizes the upper limits of neutrino fluence of anti-electron neutrinos for the low energy sample. Since there are no events observed within the search windows, the upper limits of the neutrino fluence are $4.0 \times 10^7 \text{ cm}^{-2}$ ($4.1 \times 10^7 \text{ cm}^{-2}$) selected solar flares occurring on SK-I (SK-II and SK-IV).

For the high energy sample, we considered interactions of all neutrino flavors because the distance between the Sun and the Earth is sufficiently long compared with the oscillation length of neutrinos whose energy is less than 100 GeV (Fogli et al. 2006). The flavor ratio of solar-flare neutrinos at the

Table 6. A summary of the upper limits of neutrino fluence of anti-electron neutrinos for the low energy sample. We assumed the neutrino energy spectrum from [Fargion & Moscato \(2003\)](#) and that IBD is the dominant reaction for reconstructed positron energies below 100 MeV. As described in [Okamoto et al. \(2020\)](#), for the solar flare on September 9th, 2005, the brightening of its soft X-ray light curve was relatively slow and the time derivative of the curve was not large enough. Due to this unexpected behavior, the time window for this solar flare was determined using the soft X-ray light curve directly instead of its derivative. Owing to such treatment, the duration of the search window is much longer than others and this results in the higher background rate.

Side (Channel)	Date of flare [UTC]	Observed event within window	Expected background within window	Neutrino fluence [$\text{cm}^{-2} \text{ flare}^{-1}$]
Visible (Line γ -rays)	2002 Jul. 23	No SK data	–	–
	2003 Nov. 2	0	0.0029	$< 4.0 \times 10^7$
	2005 Jan. 20	0	0.0035	$< 4.0 \times 10^7$
	1997 Nov. 6	0	0.0004	$< 4.0 \times 10^7$
	2000 Jul. 14	0	0.0027	$< 4.0 \times 10^7$
	2001 Apr. 2	0	0.0025	$< 4.0 \times 10^7$
	2001 Apr. 6	0	0.0012	$< 4.0 \times 10^7$
	2001 Apr. 15	0	0.0010	$< 4.0 \times 10^7$
	2001 Aug. 25	No SK data	–	–
	2001 Dec. 13	No SK data	–	–
	2002 Jul. 23	No SK data	–	–
	2003 Oct. 23	0	0.0022	$< 4.1 \times 10^7$
	2003 Oct. 28	0	0.0016	$< 4.1 \times 10^7$
Visible (Soft X-ray derivative)	2003 Oct. 29	0	0.0016	$< 4.1 \times 10^7$
	2003 Nov. 2	0	0.0019	$< 4.1 \times 10^7$
	2003 Nov. 4	0	0.0026	$< 4.1 \times 10^7$
	2005 Jan. 20	0	0.0025	$< 4.1 \times 10^7$
	2005 Sep. 7	0	0.0023	$< 4.1 \times 10^7$
	2005 Sep. 8	0	0.0011	$< 4.1 \times 10^7$
	2005 Sep. 9	0	0.018	$< 4.1 \times 10^7$
	2006 Dec. 5	0	0.0016	$< 4.1 \times 10^7$
	2006 Dec. 6	0	0.0008	$< 4.1 \times 10^7$
	2011 Aug. 9	0	0.0007	$< 4.1 \times 10^7$
	2012 Mar. 7	0	0.0029	$< 4.1 \times 10^7$
	2017 Sep. 6	0	0.0012	$< 4.1 \times 10^7$
	2017 Sep. 10	0	0.0024	$< 4.1 \times 10^7$
		2001 Apr. 18	0	0.016
	2002 Jul. 18	No SK data	–	–
	2002 Jul. 19	No SK data	–	–
Invisible	2003 Nov. 2	0	0.016	$< 4.1 \times 10^7$
	2003 Nov. 7	0	0.016	$< 4.1 \times 10^7$
	2003 Nov. 9	0	0.016	$< 4.1 \times 10^7$
	2005 Jul. 24	0	0.016	$< 4.1 \times 10^7$
	2011 Jun. 4	0	0.016	$< 4.1 \times 10^7$
	2012 Jul. 23	0	0.016	$< 4.1 \times 10^7$
	2014 Dec. 13	0	0.016	$< 4.1 \times 10^7$

production point is $\nu_e : \nu_\mu : \nu_\tau = 1 : 2 : 0$ due to their origin from π^\pm and μ^\pm decay while the flavor ratio at the detector is approximately $\nu_e : \nu_\mu : \nu_\tau = 1 : 1 : 1$ (Choubey & Rodejohann 2009), where we also assume that the ratio of neutrino to anti-neutrino is approximately equal, as $\nu : \bar{\nu} = 1 : 1$. The fluence upper limit for solar-flare neutrinos using the high energy sample can be obtained using a similar procedure as for the low energy sample. The difference in the calculation procedure between them is the definition of the probability density function for the number of observed events. In the high energy sample it is defined as follows:

$$P_{\text{high}}(S + B|n_{\text{obs}}) = \frac{1}{A'} \iiint \frac{e^{-(S+B)}(S+B)^{n_{\text{obs}}}}{n_{\text{obs}}!} P(\sigma(E_\nu)) P(\varepsilon_{\text{high}}^{\text{Fargion}}) P(B) d\sigma(E_\nu) d\varepsilon_{\text{high}}^{\text{Fargion}} dB, \quad (7)$$

$$\text{and } S = N_T \int dE_\nu \sum_{i=e,\mu,\tau,\bar{e},\bar{\mu},\bar{\tau}} \left(\frac{F(E_{\nu_i}) \sigma(E_{\nu_i}) \varepsilon_{\text{high}}^{\text{Fargion}}(E_{\nu_i})}{6} \right), \quad (8)$$

where A' is a normalization factor representing the total integral of $P(S+B|n_{\text{obs}})$, N_T is the number of target nuclei in the detector's fiducial volume relevant to the neutrino interactions, $\sigma(E_\nu)$ is the combined cross section for all interactions, and $\varepsilon_{\text{high}}^{\text{Fargion}}(E_\nu)$ is the event selection efficiency of the high energy sample as defined in Section 3. The systematic uncertainty of the total cross section ($\delta_{\sigma(E_\nu)}$) is estimated by the difference between two theoretical models from Smith & Moniz (1972) and from Nieves et al. (2004). For the other systematic uncertainties ($\delta_{\varepsilon_{\text{high}}}$ and ε_B), the same procedure as for the low energy sample was performed.

Table 7 summarizes the fluence limits of all detectable flavors for the high energy sample. The upper limits of neutrino fluence at 90% C.L. for solar flares occurring on the visible side of the Sun without neutrino candidates is $7.3 \times 10^5 \text{ cm}^{-2}$. The upper limit for solar flares with one neutrino candidate, which occurred on November 4th, 2003 (September 6th, 2017), is $1.1 \times 10^6 \text{ cm}^{-2}$ ($1.2 \times 10^6 \text{ cm}^{-2}$). For the solar flares occurring on the invisible side of the Sun, the upper limits of neutrino fluence at 90% C.L. are $7.3 \times 10^5 \text{ cm}^{-2}$, $1.1 \times 10^6 \text{ cm}^{-2}$, and $1.6 \times 10^6 \text{ cm}^{-2}$ for solar flares with zero, one and two neutrino candidates, respectively.

In order to calculate the upper limit with each theoretical model, $F(E_\nu)$ in Eq. (8) is replaced by the other flux predictions from Kocharov et al. (1991) and Takeishi et al. (2013) and the selection efficiencies are also evaluated with the replaced predictions. Figure 11 shows the comparison between the upper limits of neutrino fluence and the predicted neutrino fluence from three theoretical models. From the results, the SK data experimentally excluded the model of Fargion & Moscato (2003) even though this model expects several interactions in the SK detector when a energetic solar flare occurs on the invisible side of the Sun as listed in Table 1. However, the upper limits assuming the neutrino spectra from Kocharov et al. (1991) and Takeishi et al. (2013) are still higher than their predictions. As a future prospect, the model from Kocharov et al. (1991) will be tested by the next generation of neutrino detectors with significantly larger target volumes. The model of Takeishi et al. (2013), however, may be difficult to test even with the next generation of neutrino detectors.

5.2. Model-independent solar-flare neutrino fluences

As explained in Section 2.2, the excess of events reported by the Homestake experiment originally suggested the existence of solar-flare neutrinos. From this result experimental searches for solar-flare neutrinos have mainly been made by the neutrino detectors in the energy region below 100 MeV. It

Table 7. A summary of fluence limits of all detectable flavors for the high energy sample. We assumed the energy spectrum from [Fargion & Moscato \(2003\)](#) and the neutrino interaction model from [Hayato & Pickering \(2021\)](#). The higher background rate for the solar flare on September 9th, 2005 is described in the caption of Table 6.

Side (Channel)	Date of flare [UTC]	Observed event within window	Expected background within window	Neutrino fluence [$\text{cm}^{-2} \text{flare}^{-1}$]
Visible (Line γ -rays)	2002 Jul. 23	No SK data	–	–
	2003 Nov. 2	0	0.11	$< 7.3 \times 10^5$
	2005 Jan. 20	0	0.14	$< 7.3 \times 10^5$
	1997 Nov. 6	0	0.04	$< 7.3 \times 10^5$
	2000 Jul. 14	0	0.20	$< 7.3 \times 10^5$
	2001 Apr. 2	0	0.20	$< 7.3 \times 10^5$
	2001 Apr. 6	0	0.10	$< 7.3 \times 10^5$
	2001 Apr. 15	0	0.08	$< 7.3 \times 10^5$
	2001 Aug. 25	No SK data	–	–
	2001 Dec. 13	No SK data	–	–
	2002 Jul. 23	No SK data	–	–
	2003 Oct. 23	0	0.16	$< 7.3 \times 10^5$
	2003 Oct. 28	0	0.12	$< 7.3 \times 10^5$
	2003 Oct. 29	0	0.12	$< 7.3 \times 10^5$
	Visible (Soft X-ray derivative)	2003 Nov. 2	0	0.14
2003 Nov. 4		1	0.20	$< 1.1 \times 10^6$
2005 Jan. 20		0	0.18	$< 7.3 \times 10^5$
2005 Sep. 7		0	0.18	$< 7.3 \times 10^5$
2005 Sep. 8		0	0.08	$< 7.3 \times 10^5$
2005 Sep. 9		0	0.67	$< 7.3 \times 10^5$
2006 Dec. 5		0	0.12	$< 7.3 \times 10^5$
2006 Dec. 6		0	0.06	$< 7.3 \times 10^5$
2011 Aug. 9		0	0.06	$< 7.3 \times 10^5$
2012 Mar. 7		0	0.20	$< 7.3 \times 10^5$
2017 Sep. 6		1	0.12	$< 1.2 \times 10^6$
2017 Sep. 10		0	0.18	$< 7.3 \times 10^5$
Invisible		2001 Apr. 18	0	0.62
	2002 Jul. 18	No SK data	–	–
	2002 Jul. 19	No SK data	–	–
	2003 Nov. 2	0	0.62	$< 7.3 \times 10^5$
	2003 Nov. 7	2	0.62	$< 1.6 \times 10^6$
	2003 Nov. 9	0	0.62	$< 7.3 \times 10^5$
	2005 Jul. 24	2	0.62	$< 1.6 \times 10^6$
	2011 Jun. 4	1	0.62	$< 1.1 \times 10^6$
	2012 Jul. 23	1	0.62	$< 1.1 \times 10^6$
	2014 Dec. 13	0	0.62	$< 7.3 \times 10^5$

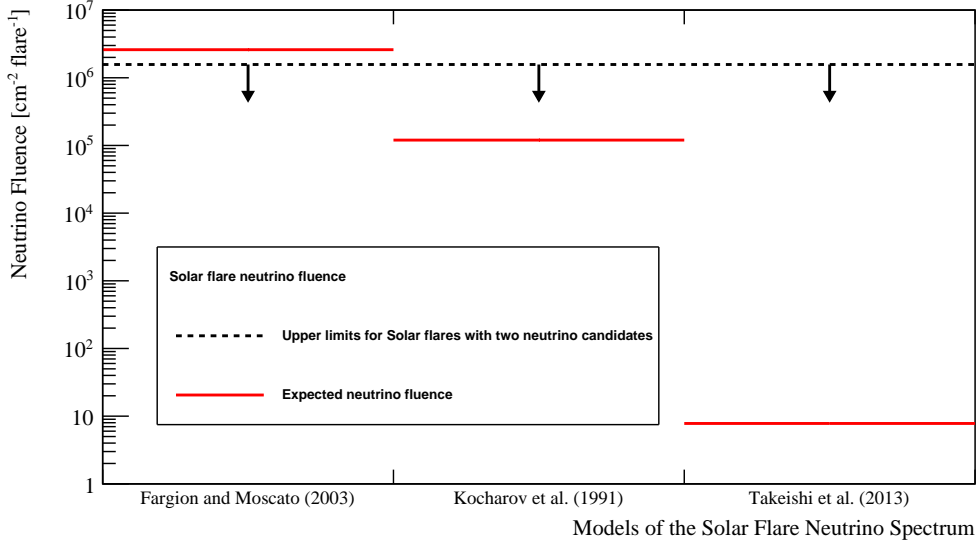


Figure 11. The comparison between upper limits of neutrino fluence considering neutrino spectra from the specific theoretical models of [Kocharov et al. \(1991\)](#), [Fargion \(2004\)](#), and [Takeishi et al. \(2013\)](#), and their predicted fluences. The black dashed lines with downward arrows (red solid lines) show the upper limit of neutrino fluence (expected neutrino fluence based on each theoretical model). The upper limits are conservatively calculated by considering two neutrino candidates detected within the search windows.

should be noted that past studies by the SNO ([Aharmim et al. 2014](#)), Borexino ([Agostini et al. 2021](#)), and KamLAND ([Abe et al. 2022b](#)) experiments searched for neutrinos from solar flares in coincidence with the soft X-ray light curves recorded by the GOES satellite, including solar flares with smaller intensity, such as M-class flares. Due to the different assumptions and samples of selected solar flares, we cannot directly compare previous experimental results with the results presented in this article. To compare these results with those from other experiments, the upper limit of neutrino fluence without considering a specific model was also calculated using the low energy sample. In this case, the probability density function at a neutrino energy E is defined as follows:

$$P_{\text{low}}(S + B | n_{\text{obs}})(E) = \frac{1}{A} \iiint \frac{e^{-(S(E)+B)} (S(E) + B)^{n_{\text{obs}}}}{n_{\text{obs}}!} P(\sigma_{\text{IBD}}) P(\varepsilon_{\text{low}}^{\text{Ind}}) P(B) d\sigma_{\text{IBD}} d\varepsilon_{\text{low}}^{\text{Ind}} dB, \quad (9)$$

$$\text{and } S(E) = N_p t_{\text{emit}} \int F(E_\nu) \theta(E, E_\nu) \sigma_{\text{IBD}}(E_\nu) \varepsilon_{\text{low}}^{\text{Ind}} dE_\nu \quad (10)$$

where $\varepsilon_{\text{low}}^{\text{Ind}}$ is the selection efficiency listed in Table 2, $\theta(E, E_\nu)$ is a step function which is defined as,

$$\theta(E, E_\nu) = \begin{cases} 1 & (E - 5 \text{ MeV} < E_\nu \leq E + 5 \text{ MeV}), \\ 0 & (\text{otherwise}), \end{cases} \quad (11)$$

and the other variables and functions are the same as those used in Eq. (4). To convert from the reconstructed positron energy to the incoming electron anti-neutrino energy the theoretical model of [Strumia & Vissani \(2003\)](#) is used. To address the effect of energy resolution and the energy of the

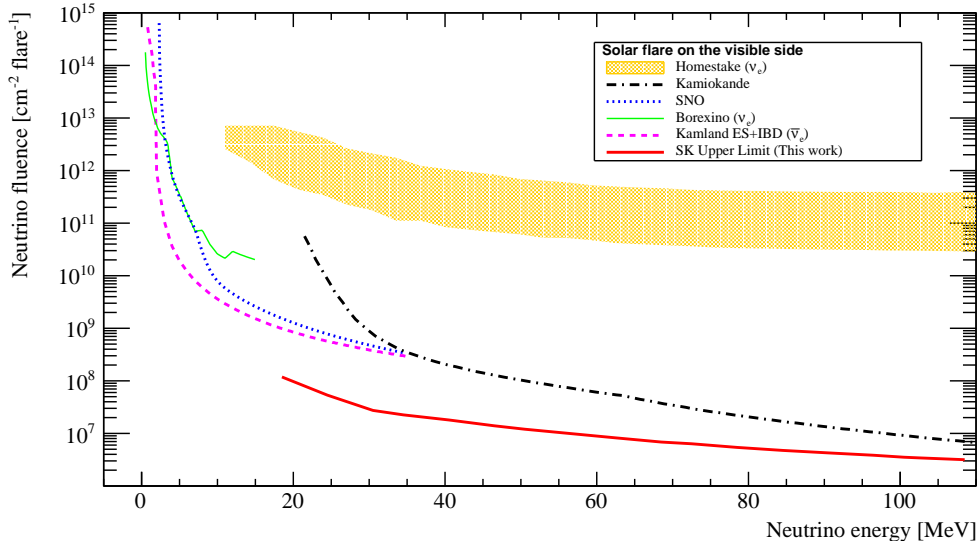


Figure 12. The upper limit of neutrino fluence from the data taken by SK-I, II, III, and IV (red thick-solid) together with the other experimental results. The orange contour shows the allowed parameter region from the Homestake experiment (Davis 1994). Black long-dashed-dotted, blue dotted, green thin-solid, and pink dashed lines show the upper limits from Kamiokande (Hirata et al. 1988), SNO (Aharmim et al. 2014), Borexino (Agostini et al. 2021), and KamLAND (Abe et al. 2022b) experiments, respectively.

simultaneously produced neutron, the data in the neutrino energy range from 20 to 110 MeV was analyzed and the upper limit of neutrino fluence calculated every 10 MeV.

Figure 12 shows the SK result for the upper limit of neutrino fluence without considering a specific theoretical model, together with other experimental results (Davis 1994; Hirata et al. 1988; Aharmim et al. 2014; Agostini et al. 2021; Abe et al. 2022b). Comparing to other experimental limits of neutrino fluence, the SK limit is improved by at least an order of magnitude in the energy region from 20 to 110 MeV. The SK limit fully excludes the allowed parameter region which was favored by the Homestake experiment (Davis 1994) and gives a strong constraint for neutrino fluence from powerful solar flares.

5.3. Energy conversion factor

As explained in Section 2.1, Fargion & Moscato (2003) estimated the number of interactions in the SK detector by introducing the conversion factor η in Eq. (1). The experimental search for solar-flare neutrinos by the SK detector gives a constraint on this parameter. However, estimating the total energy of a solar flare is difficult because the magnetic energy released in a solar flare is converted into a variety of different forms. Accordingly, the estimation of total energy is performed for a limited number of solar flares.

By considering the selection efficiencies of each sample and the energies of powerful solar flares, the conversion factor is calculated based on the number of observed events in each sample. For the high energy sample, we used Eq. (1) as the number of interactions. For the low energy sample, we used the following equation, since Fargion (2004) also estimated the number of interactions only using the

Table 8. A summary of the upper limits of the conversion factor η . The estimated energies of selected solar flares are taken from [Emslie et al. \(2004\)](#), [Kane et al. \(2005\)](#), [Aschwanden et al. \(2014\)](#), [Aschwanden et al. \(2015\)](#), and [Motorina et al. \(2020\)](#). Note that their flare energies are estimated using different forms of energy, i.e. magnetic energy in [Emslie et al. \(2004\)](#) and [Motorina et al. \(2020\)](#), total released energy by electrons more than 20 keV in [Kane et al. \(2005\)](#), thermal energy in [Aschwanden et al. \(2015\)](#), and magnetic potential energy in [Aschwanden et al. \(2014\)](#), respectively.

Date of flare	Estimated energy of solar flare [erg]	Reference for estimated energy	η_{low}	η_{high}
2002 Jul. 23	$10^{32.3}$	Emslie et al. (2004)	No SK data	
2003 Oct. 28	$10^{32.3}$	Emslie et al. (2004)	< 0.16	< 0.025
2003 Nov. 4	1.3×10^{34}	Kane et al. (2005)	< 0.0025	< 0.0006
2011 Aug. 9	1.29×10^{32}	Aschwanden et al. (2015)	< 0.095	< 0.038
2012 Mar. 7	1.74×10^{33}	Aschwanden et al. (2014)	< 0.018	< 0.0028
2017 Sep. 6	5.6×10^{32}	Motorina et al. (2020)	< 0.022	< 0.014

IBD reaction,

$$n_{\text{int}}^{\text{IBD}} = \left[0.63 \left(\frac{\bar{E}_{\bar{\nu}_e}}{35 \text{ MeV}} \right) + 1.58 \right] \eta \left(\frac{E_{\text{FL}}}{10^{31} \text{ erg}} \right), \quad (12)$$

where $n_{\text{int}}^{\text{IBD}}$ is the number of IBD interactions in the SK detector, $\bar{E}_{\bar{\nu}_e}$ is the average energy of the electron anti-neutrino spectrum derived from [Fargion \(2004\)](#), the first, and the second terms in the square bracket are the number of interactions in the energy range of 10–100 MeV, and 100 MeV–1 GeV, respectively⁷. Table 7 summarizes the 90% C.L. upper limits of the conversion factors, η_{low} for the low energy sample and η_{high} for the high energy sample, from the most powerful solar flares during solar cycle 23 and 24.

In the case of the solar flare that occurred on November 4th, 2003, [Kane et al. \(2005\)](#) estimated the total energy released as 1.3×10^{34} ergs by analyzing electrons above 20 keV. By analyzing the high (low) energy sample the conversion factor η was found to be < 0.0006 (< 0.0025) at 90% C.L. These conversion factors are at least 10^3 smaller than the assumption from [Fargion & Moscato \(2003\)](#). Hence, this result suggests that the conversion factor introduced in [Fargion & Moscato \(2003\)](#) is too optimistic an assumption for the energy transfer that produces neutrinos during the solar flare.

6. SUMMARY AND FUTURE PROSPECTS

Neutrinos from solar flares are necessary to understand the mechanisms of proton acceleration at the astrophysical site. For solar flares that occurred on the visible and invisible sides of the Sun, we first estimated the time of neutrino emission using optical light curves and CME observations by solar satellites. We then searched for neutrino events in the Super-Kamiokande detector coincident with these solar flares. Two neutrino events were observed coincident with solar flares that occurred on the visible side of the Sun while six neutrino events were observed coincident with solar flares that occurred on the invisible side of the Sun. All of them are consistent with the background rate under

⁷ The expected number of interactions above 1 GeV is estimated to be 4.9% by calculating the anti-electron neutrino spectrum from [Fargion & Moscato \(2003\)](#) and the IBD cross section from [Strumia & Vissani \(2003\)](#). We ignored this contribution because other uncertainties, such as the total energy of the solar flare, and the fluctuation of the background event rate in the low energy sample exist in this analysis.

the usual operation of the SK detector. Based on the observed events within the search window we obtained upper limits of the neutrino fluence depending on the assumed theoretical neutrino production model. For example, the fluence limit for the largest solar flare of class X28.0 that occurred at the visible side of the Sun on the November 4th, 2003 is $1.1 \times 10^6 \text{ cm}^{-2}$. In addition, the fluence limit for the solar flare that occurred on the invisible side of the Sun on November 7th, 2003, which followed the largest solar flare, is $1.6 \times 10^6 \text{ cm}^{-2}$. From the obtained fluences, the upper limits on the energy conversion factor were estimated based on [Fargion & Moscato \(2003\)](#). In the case of the largest solar flare on November 4th, 2003, $\eta < 0.0006$ at 90% C.L., which is two orders of magnitude smaller than the estimate of [Fargion & Moscato \(2003\)](#). Therefore, this experimental result suggests that the theoretical assumption of energy conversion during solar flares should be reconsidered.

In order to compare these results with other experimental searches, the fluence limit below 100 MeV was also obtained without considering a specific theoretical model. The SK result is the most stringent constraint on the neutrino fluence from solar flares in the MeV region to date.

In July 2020, 13 tonnes of $\text{Gd}_2(\text{SO}_4)_3 \cdot 8\text{H}_2\text{O}$ (gadolinium sulfate octahydrate) were dissolved into the SK water tank in order to improve its neutron detection efficiency ([Abe et al. 2022a](#)), followed by an additional 26 tonnes in June 2022. The main motivation for the gadolinium loading is to increase the detector's sensitivity to diffuse supernova electron anti-neutrinos. This technique also enhances the sensitivity to solar-flare neutrinos as well. In addition to the SK phases with Gd, further searches to understand the production of solar-flare neutrinos should be performed by large scale neutrino detectors such as Hyper-Kamiokande ([Abe et al. 2018b](#)), IceCube gen-2 ([Aartsen et al. 2021](#)), and JUNO ([Adam et al. 2015](#)) during solar cycle 25 that started from late 2019.

We thank D. Fargion from the Sapienza University of Rome for providing the expected fluence of neutrinos from solar flares. We also thank S. Masuda from Institute for Space-Earth Environmental Research, Nagoya University, T. Terasawa from the institute for cosmic ray research, the University of Tokyo, and S. Yashiro from Catholic University of America, for valuable discussion related with the search windows determination at the both visible and invisible sides of the Sun.

We gratefully acknowledge the cooperation of the Kamioka Mining and Smelting Company. The Super-Kamiokande experiment has been built and operated from funding by the Japanese Ministry of Education, Culture, Sports, Science and Technology, the U.S. Department of Energy, and the U.S. National Science Foundation. Some of us have been supported by funds from the National Research Foundation of Korea NRF-2009-0083526 (KNRC) funded by the Ministry of Science, ICT, and Future Planning and the Ministry of Education (2018R1D1A1B07049158, 2021R1I1A1A01059559), the Japan Society for the Promotion of Science, the National Natural Science Foundation of China under Grants No.11620101004, the Spanish Ministry of Science, Universities and Innovation (grant PGC2018-099388-B-I00), the Natural Sciences and Engineering Research Council (NSERC) of Canada, the Scinet and Westgrid consortia of Compute Canada, the National Science Centre (UMO-2018/30/E/ST2/00441) and the Ministry of Education and Science (DIR/WK/2017/05), Poland, the Science and Technology Facilities Council (STFC) and GridPPP, UK, the European Union's Horizon 2020 Research and Innovation Programme under the Marie Skłodowska-Curie grant agreement no.754496, H2020-MSCA-RISE-2018 JENNIFER2 grant agreement no.822070, and H2020-MSCA-RISE-2019 SK2HK grant agreement no. 872549.

This work was carried out by the joint research program of the Institute for Space-Earth Environmental Research (ISEE), Nagoya University. A part of this study was carried using the computational resources of the Center for Integrated Data Science, Institute for Space-Earth Environmental Research, Nagoya University, through the joint research program.

REFERENCES

- Aartsen, M. G., Abbasi, R., Ackermann, M., et al. 2021, *J. Phys. G*, 48, 060501, doi: [10.1088/1361-6471/abbd48](https://doi.org/10.1088/1361-6471/abbd48)
- Abbasi, R., Ackermann, M., Adams, J., et al. 2021, *PhRvD*, 103, 102001, doi: [10.1103/PhysRevD.103.102001](https://doi.org/10.1103/PhysRevD.103.102001)
- Abe, K., Hayato, Y., Iida, T., et al. 2014, *NIMPA*, 737, 253, doi: [10.1016/j.nima.2013.11.081](https://doi.org/10.1016/j.nima.2013.11.081)
- Abe, K., Haga, Y., Hayato, Y., et al. 2016, *PhRvD*, 94, 052010, doi: [10.1103/PhysRevD.94.052010](https://doi.org/10.1103/PhysRevD.94.052010)
- Abe, K., Bronner, C., Haga, Y., et al. 2018a, *PhRvD*, 97, 072001, doi: [10.1103/PhysRevD.97.072001](https://doi.org/10.1103/PhysRevD.97.072001)
- Abe, K., Abe, K., Aihara, H., et al. 2018b, arXiv e-prints, arXiv:1805.04163, <https://arxiv.org/abs/1805.04163>
- Abe, K., Bronner, C., Hayato, Y., et al. 2021, *PhRvD*, 104, 122002, doi: [10.1103/PhysRevD.104.122002](https://doi.org/10.1103/PhysRevD.104.122002)
- . 2022a, *NIMPA*, 1027, 166248, doi: [10.1016/j.nima.2021.166248](https://doi.org/10.1016/j.nima.2021.166248)
- Abe, S., Asami, S., Gando, A., et al. 2022b, *ApJ*, 924, 103, doi: [10.3847/1538-4357/ac35d1](https://doi.org/10.3847/1538-4357/ac35d1)
- Ackermann, M., Allafort, A., Baldini, L., et al. 2017, *ApJ*, 835, 219, doi: [10.3847/1538-4357/835/2/219](https://doi.org/10.3847/1538-4357/835/2/219)
- Adam, T., An, F., An, G., et al. 2015, arXiv e-prints, arXiv:1508.07166, <https://arxiv.org/abs/1508.07166>
- Aglietta, M., Badino, G., Bologna, G., et al. 1991, *ApJ*, 382, 344, doi: [10.1086/170722](https://doi.org/10.1086/170722)
- Agostini, M., et al. 2021, *APh*, 125, 102509, doi: [10.1016/j.astropartphys.2020.102509](https://doi.org/10.1016/j.astropartphys.2020.102509)

- Aharmim, B., Ahmed, S. N., Anthony, A. E., et al. 2014, *APh*, 55, 1, doi: [10.1016/j.astropartphys.2013.12.004](https://doi.org/10.1016/j.astropartphys.2013.12.004)
- Ajello, M., Baldini, L., Bastieri, D., et al. 2021, *ApJS*, 252, 13, doi: [10.3847/1538-4365/abd32e](https://doi.org/10.3847/1538-4365/abd32e)
- Andrews, M. D. 2003, *SoPh*, 218, 261, doi: [10.1023/B:SOLA.0000013039.69550.bf](https://doi.org/10.1023/B:SOLA.0000013039.69550.bf)
- Aschwanden, M. J., Boerner, P., Ryan, D., et al. 2015, *ApJ*, 802, 53, doi: [10.1088/0004-637X/802/1/53](https://doi.org/10.1088/0004-637X/802/1/53)
- Aschwanden, M. J., Xu, Y., & Jing, J. 2014, *ApJ*, 797, 50, doi: [10.1088/0004-637X/797/1/50](https://doi.org/10.1088/0004-637X/797/1/50)
- Ashie, Y., Hosaka, J., Ishihara, K., et al. 2005, *PhRvD*, 71, 112005, doi: [10.1103/PhysRevD.71.112005](https://doi.org/10.1103/PhysRevD.71.112005)
- Atwood, W. B., Abdo, A. A., Ackermann, M., et al. 2009, *ApJ*, 697, 1071, doi: [10.1088/0004-637X/697/2/1071](https://doi.org/10.1088/0004-637X/697/2/1071)
- Bahcall, J. N. 1988, *PhRvL*, 61, 2650, doi: [10.1103/PhysRevLett.61.2650](https://doi.org/10.1103/PhysRevLett.61.2650)
- Bahcall, J. N., Field, G. B., & Press, W. H. 1987, *ApJL*, 320, L69, doi: [10.1086/184978](https://doi.org/10.1086/184978)
- Bahcall, J. N., Pinsonneault, M. H., & Basu, S. 2001, *ApJ*, 555, 990, doi: [10.1086/321493](https://doi.org/10.1086/321493)
- Battistoni, G., Ferrari, A., Montaruli, T., & Sala, P. R. 2005, *Astroparticle Physics*, 23, 526, doi: [10.1016/j.astropartphys.2005.03.006](https://doi.org/10.1016/j.astropartphys.2005.03.006)
- Bays, K., Iida, T., Abe, K., et al. 2012, *PhRvD*, 85, 052007, doi: [10.1103/PhysRevD.85.052007](https://doi.org/10.1103/PhysRevD.85.052007)
- Bazilevskaya, G. A., Stozhkov, Y. I., & Charakhch'yan, T. N. 1982, *Soviet Journal of Experimental and Theoretical Physics Letters*, 35, 341
- Brueckner, G. E., Howard, R. A., Koomen, M. J., et al. 1995, *SoPh*, 162, 357, doi: [10.1007/BF00733434](https://doi.org/10.1007/BF00733434)
- Brun, R., Bruyant, F., Carminati, F., et al. 1994, doi: [10.17181/CERN.MUHF.DMJ1](https://doi.org/10.17181/CERN.MUHF.DMJ1)
- Chao, J. K., & Lepping, R. P. 1974, *J. Geophys. Res.*, 79, 1799, doi: [10.1029/JA079i013p01799](https://doi.org/10.1029/JA079i013p01799)
- Choubey, S., & Rodejohann, W. 2009, *PhRvD*, 80, 113006, doi: [10.1103/PhysRevD.80.113006](https://doi.org/10.1103/PhysRevD.80.113006)
- Chupp, E. L., Forrest, D. J., Higbie, P. R., et al. 1973, *Nature*, 241, 333, doi: [10.1038/241333a0](https://doi.org/10.1038/241333a0)
- Chupp, E. L., Forrest, D. J., Ryan, J. M., et al. 1981, *ApJL*, 244, L171, doi: [10.1086/183505](https://doi.org/10.1086/183505)
- Chupp, E. L., Debrunner, H., Flueckiger, E., et al. 1987, *ApJ*, 318, 913, doi: [10.1086/165423](https://doi.org/10.1086/165423)
- Datlowe, D. W., Hudson, H. S., & Peterson, L. E. 1974, *SoPh*, 35, 193, doi: [10.1007/BF00156967](https://doi.org/10.1007/BF00156967)
- Davis, R. 1994, *Prog. Part. Nucl. Phys.*, 32, 13, doi: [10.1016/0146-6410\(94\)90004-3](https://doi.org/10.1016/0146-6410(94)90004-3)
- de Wasseige, G. 2016, arXiv e-prints, arXiv:1606.00681, <https://arxiv.org/abs/1606.00681>
- Debrunner, H., Lockwood, J. A., Barat, C., et al. 1997, *ApJ*, 479, 997, doi: [10.1086/303895](https://doi.org/10.1086/303895)
- Domingo, V., Fleck, B., & Poland, A. I. 1995, *SoPh*, 162, 1, doi: [10.1007/BF00733425](https://doi.org/10.1007/BF00733425)
- Ellison, M. A. 1963, *QJRAS*, 4, 62
- Emslie, A. G., Kucharek, H., Dennis, B. R., et al. 2004, *Journal of Geophysical Research (Space Physics)*, 109, A10104, doi: [10.1029/2004JA010571](https://doi.org/10.1029/2004JA010571)
- Erofeeva, I. N., Liutov, S. I., Murzin, V. S., et al. 1983, in *International Cosmic Ray Conference*, Vol. 7, *International Cosmic Ray Conference*, 104
- Fargion, D. 2004, *JHEP*, 2004, 045, doi: [10.1088/1126-6708/2004/06/045](https://doi.org/10.1088/1126-6708/2004/06/045)
- Fargion, D., & Moscato, F. 2003, *Chinese Journal of Astronomy and Astrophysics Supplement*, 3, 75, doi: [10.1088/1009-9271/3/S1/75](https://doi.org/10.1088/1009-9271/3/S1/75)
- Fletcher, L., & Hudson, H. S. 2008, *ApJ*, 675, 1645, doi: [10.1086/527044](https://doi.org/10.1086/527044)
- Fogli, G. L., Lisi, E., Mirizzi, A., Montanino, D., & Serpico, P. D. 2006, *PhRvD*, 74, 093004, doi: [10.1103/PhysRevD.74.093004](https://doi.org/10.1103/PhysRevD.74.093004)
- Forrest, D. J., Vestrand, W. T., Chupp, E. L., et al. 1986, *Advances in Space Research*, 6, 115, doi: [10.1016/0273-1177\(86\)90127-4](https://doi.org/10.1016/0273-1177(86)90127-4)
- Fukuda, S., Fukuda, Y., Hayakawa, T., et al. 2003, *NIMPA*, 501, 418, doi: [10.1016/S0168-9002\(03\)00425-X](https://doi.org/10.1016/S0168-9002(03)00425-X)
- Gando, A., Gando, Y., Ichimura, K., et al. 2012, *ApJ*, 745, 193, doi: [10.1088/0004-637X/745/2/193](https://doi.org/10.1088/0004-637X/745/2/193)
- Gopalswamy, N., Akiyama, S., & Yashiro, S. 2009, in *Universal Heliophysical Processes*, ed. N. Gopalswamy & D. F. Webb, Vol. 257, 283–286, doi: [10.1017/S174392130902941X](https://doi.org/10.1017/S174392130902941X)
- Gosling, J. T., Hildner, E., MacQueen, R. M., et al. 1975, *SoPh*, 40, 439, doi: [10.1007/BF00162390](https://doi.org/10.1007/BF00162390)
- Hayato, Y., & Pickering, L. 2021, *European Physical Journal Special Topics*, 230, 4469, doi: [10.1140/epjs/s11734-021-00287-7](https://doi.org/10.1140/epjs/s11734-021-00287-7)

- Hirata, K. S., Kajita, T., Kifune, T., et al. 1988, *PhRvL*, 61, 2653, doi: [10.1103/PhysRevLett.61.2653](https://doi.org/10.1103/PhysRevLett.61.2653)
- . 1990, *ApJ*, 359, 574, doi: [10.1086/169088](https://doi.org/10.1086/169088)
- Horiuchi, S., Beacom, J. F., & Dwek, E. 2009, *PhRvD*, 79, 083013, doi: [10.1103/PhysRevD.79.083013](https://doi.org/10.1103/PhysRevD.79.083013)
- Hudson, H., & Ryan, J. 1995, *ARA&A*, 33, 239, doi: [10.1146/annurev.aa.33.090195.001323](https://doi.org/10.1146/annurev.aa.33.090195.001323)
- Hundhausen, A. J., Stanger, A. L., & Serbicki, S. A. 1994, in *ESA Special Publication*, Vol. 373, *Solar Dynamic Phenomena and Solar Wind Consequences, the Third SOHO Workshop*, ed. J. J. Hunt, 409
- Kaiser, M. L., Kucera, T. A., Davila, J. M., et al. 2008, *SSRv*, 136, 5, doi: [10.1007/s11214-007-9277-0](https://doi.org/10.1007/s11214-007-9277-0)
- Kanbach, G., Bertsch, D. L., Fichtel, C. E., et al. 1993, *A&AS*, 97, 349
- Kane, S. R. 1974, in *Coronal Disturbances*, ed. G. A. Newkirk, Vol. 57, 105
- Kane, S. R., McTiernan, J. M., & Hurley, K. 2005, *A&A*, 433, 1133, doi: [10.1051/0004-6361:20041875](https://doi.org/10.1051/0004-6361:20041875)
- Karlický, M., & Kosugi, T. 2004, *A&A*, 419, 1159, doi: [10.1051/0004-6361:20034323](https://doi.org/10.1051/0004-6361:20034323)
- Kocharov, G. E., Koval'Tsov, G. A., & Usoskin, I. G. 1991, *NCimC*, 14, 417, doi: [10.1007/BF02509184](https://doi.org/10.1007/BF02509184)
- Kolbe, E., Langanke, K., & Vogel, P. 2002, *PhRvD*, 66, 013007, doi: [10.1103/PhysRevD.66.013007](https://doi.org/10.1103/PhysRevD.66.013007)
- Krucker, S., Hudson, H. S., Glesener, L., et al. 2010, *ApJ*, 714, 1108, doi: [10.1088/0004-637X/714/2/1108](https://doi.org/10.1088/0004-637X/714/2/1108)
- Kurt, V. G., Yushkov, B. Y., Kudela, K., & Galkin, V. I. 2010, *Cosmic Research*, 48, 70, doi: [10.1134/S0010952510010053](https://doi.org/10.1134/S0010952510010053)
- Leikov, N. G., Akimov, V. V., Volzhenskaia, V. A., et al. 1993, *A&AS*, 97, 345
- Lemen, J. R., Duncan, D. W., Edwards, C. G., et al. 2004, in *Society of Photo-Optical Instrumentation Engineers (SPIE) Conference Series*, Vol. 5171, *Telescopes and Instrumentation for Solar Astrophysics*, ed. S. Fineschi & M. A. Gummin, 65–76, doi: [10.1117/12.507566](https://doi.org/10.1117/12.507566)
- Lin, R. P., Dennis, B. R., Hurford, G. J., et al. 2002, *SoPh*, 210, 3, doi: [10.1023/A:1022428818870](https://doi.org/10.1023/A:1022428818870)
- Liu, W., Petrosian, V., Dennis, B. R., & Jiang, Y. W. 2008, *ApJ*, 676, 704, doi: [10.1086/527538](https://doi.org/10.1086/527538)
- Masuda, S., Kosugi, T., Hara, H., Tsuneta, S., & Ogawara, Y. 1994, *Nature*, 371, 495, doi: [10.1038/371495a0](https://doi.org/10.1038/371495a0)
- Moon, Y. J., Choe, G. S., Wang, H., et al. 2002, *ApJ*, 581, 694, doi: [10.1086/344088](https://doi.org/10.1086/344088)
- Motorina, G. G., Lysenko, A. L., Anfinogentov, S. A., & Fleishman, G. D. 2020, *Geomagnetism and Aeronomy*, 60, 929, doi: [10.1134/S001679322007018X](https://doi.org/10.1134/S001679322007018X)
- Nakajima, H., Kosugi, T., Kai, K., & Enome, S. 1983, *Nature*, 305, 292, doi: [10.1038/305292a0](https://doi.org/10.1038/305292a0)
- Nakano, Y., Hokama, T., Matsubara, M., et al. 2020, *NIMPA*, 977, 164297, doi: [10.1016/j.nima.2020.164297](https://doi.org/10.1016/j.nima.2020.164297)
- Narukage, N., Shimojo, M., & Sakao, T. 2014, *ApJ*, 787, 125, doi: [10.1088/0004-637X/787/2/125](https://doi.org/10.1088/0004-637X/787/2/125)
- Nieves, J., Amaro, J. E., & Valverde, M. 2004, *PhRvC*, 70, 055503, doi: [10.1103/PhysRevC.70.055503](https://doi.org/10.1103/PhysRevC.70.055503)
- Okamoto, K., Nakano, Y., Masuda, S., et al. 2020, *SoPh*, 295, 133, doi: [10.1007/s11207-020-01706-z](https://doi.org/10.1007/s11207-020-01706-z)
- Ramaty, R., Kozlovsky, B., & Lingenfelter, R. E. 1975, *SSRv*, 18, 341, doi: [10.1007/BF00212911](https://doi.org/10.1007/BF00212911)
- Richard, E., Okumura, K., Abe, K., et al. 2016, *PhRvD*, 94, 052001, doi: [10.1103/PhysRevD.94.052001](https://doi.org/10.1103/PhysRevD.94.052001)
- Roe, B. P., & Woodroffe, M. B. 2000, *PhRvD*, 63, 013009, doi: [10.1103/PhysRevD.63.013009](https://doi.org/10.1103/PhysRevD.63.013009)
- Smith, D. M., Share, G. H., Murphy, R. J., et al. 2003, *ApJL*, 595, L81, doi: [10.1086/378173](https://doi.org/10.1086/378173)
- Smith, R. A., & Moniz, E. J. 1972, *Nucl. Phys. B*, 43, 605, doi: [10.1016/0550-3213\(75\)90612-4](https://doi.org/10.1016/0550-3213(75)90612-4)
- Strumia, A., & Vissani, F. 2003, *PhLB*, 564, 42, doi: [10.1016/S0370-2693\(03\)00616-6](https://doi.org/10.1016/S0370-2693(03)00616-6)
- Takeishi, R., Terasawa, T., & Kotoku, J. 2013, in *International Cosmic Ray Conference*, Vol. 33, *International Cosmic Ray Conference*, 3656
- Takenaka, A., Abe, K., Bronner, C., et al. 2020, *PhRvD*, 102, 112011, doi: [10.1103/PhysRevD.102.112011](https://doi.org/10.1103/PhysRevD.102.112011)
- Tsuneta, S., & Naito, T. 1998, *ApJL*, 495, L67, doi: [10.1086/311207](https://doi.org/10.1086/311207)
- Vourlidis, A., Howard, R. A., Esfandiari, E., et al. 2010, *ApJ*, 722, 1522, doi: [10.1088/0004-637X/722/2/1522](https://doi.org/10.1088/0004-637X/722/2/1522)

- Watanabe, K., Gros, M., Stoker, P. H., et al. 2006, ApJ, 636, 1135, doi: [10.1086/498086](https://doi.org/10.1086/498086)
- Yamada, S., et al. 2010, IEEE Trans. Nucl. Sci., 57, 428, doi: [10.1109/TNS.2009.2034854](https://doi.org/10.1109/TNS.2009.2034854)
- Yashiro, S., & Gopalswamy, N. 2009, in Universal Heliophysical Processes, ed. N. Gopalswamy & D. F. Webb, Vol. 257, 233–243, doi: [10.1017/S1743921309029342](https://doi.org/10.1017/S1743921309029342)
- Yashiro, S., Gopalswamy, N., Michalek, G., et al. 2004, Journal of Geophysical Research (Space Physics), 109, A07105, doi: [10.1029/2003JA010282](https://doi.org/10.1029/2003JA010282)
- Yoshimori, M. 1984, Journal of the Physical Society of Japan, 53, 4499, doi: [10.1143/JPSJ.53.4499](https://doi.org/10.1143/JPSJ.53.4499)
- Zhang, Y., et al. 2016, PhRvD, 93, 012004, doi: [10.1103/PhysRevD.93.012004](https://doi.org/10.1103/PhysRevD.93.012004)

APPENDIX

A. SEARCH WINDOWS FOR NEUTRINOS FROM INVISIBLE SIDE OF THE SUN

As discussed in Section 2.4, the searches for neutrinos associated from solar flares occurring at the invisible side provide information about acceleration mechanism of downward going proton flux. However, no satellite, except for a limited number of planet explorers, directly monitors an explosive phenomenon at the invisible side before the launch of STEREO⁸ satellites on 2006 (Kaiser et al. 2008).

Andrews (2003) found the association rate of CMEs with solar flares clearly increases with the flare's peak flux of soft X-rays, fluence, and time duration. Hence, an occurrence time of CMEs is helpful to estimate the time of powerful solar flare occurring on the invisible side of the Sun instead of the data taken by limited number of planet explorers.

The catalog of CMEs observed by the SOHO spacecraft are maintained by NASA (Yashiro et al. 2004)⁹ and this catalog summarizes the time of CMEs emission and its location.

Moon et al. (2002) and Yashiro & Gopalswamy (2009) statistically examined a possible correlation between the kinetic energy of CMEs and the intensity of the solar flare monitored by GOES satellite and found the weak positive correlation between them. Based on that studies, we conservatively determined the threshold as 2000 km s^{-1} in order to select solar flares classified to X class. This criterion roughly corresponds to solar flares with X2.0¹⁰. By this method, ten CMEs across solar cycles 23 and 24 were selected and Table 9 summarizes their dates, times, locations, and speeds of CMEs.

Yashiro & Gopalswamy (2009) also investigated the time difference between the CMEs and the solar flares. That study found the standard deviation of their time difference is 1020 s from its distribution. For covering the time of neutrino production during solar flares, we set the start time as 3060 s before the time of CMEs, which corresponds to three standard deviations of their time difference. For the end time, we conservatively set the duration of 4178 s after the time of CMEs, where this duration is determined in Okamoto et al. (2020) from the light curve of soft X-ray recorded by the GOES satellite since all processes, such as acceleration, energy release, and etc, occurring during a solar flare, is likely to complete within this time duration. Finally, the search window for all solar flare occurred on the invisible side of the Sun is 7238 s in total. Table 9 also summarizes the times of corresponding search window for solar-flare neutrinos from the invisible side of the Sun.

B. EVENT DISPLAY AND SKYMAP OF THE OBSERVED EVENTS FROM SOLAR FLARES ON THE VISIBLE SIDE

The SK event displays of neutrino candidates from solar flares on the visible side of the Sun and sky maps together with the location of the Sun are shown in Figures 13 and 14.

⁸ Solar Terrestrial Relations Observatory

⁹ https://cdaw.gsfc.nasa.gov/CME_list/

¹⁰ Note that some flares without CMEs are reported when its class is less than X1.6 (Gopalswamy et al. 2009).

Table 9. The summary of the search windows estimated in this study for energetic CMEs occurred at the invisible side of the Sun. The date, time, and active region (AR) are taken from SOHO LASCO CME CATALOG (Yashiro et al. 2004).

Date	Time [UTC]	t_{start}	t_{end}	AR location	Speed [km s^{-1}]
2001 Apr. 18	02:06:24	01:15:24	03:16:02	SW90b	2464.2
2002 Jul. 18	18:58:20	18:07:20	20:07:58	E90b	2191.3
2002 Jul. 19	16:04:34	15:13:34	17:14:12	S15E90	2046.6
2003 Nov. 2	09:00:23	15:13:34	17:14:12	SW90b	2036.0
2003 Nov. 7	15:32:19	14:41:19	16:41:57	W90b	2237.0
2003 Nov. 9	05:57:57	05:06:57	07:45:29	E90b	2008.1
2005 Jul. 24	13:35:51	12:44:51	14:45:29	E90b	2527.8
2011 Jun. 4	21:42:42	20:51:42	22:52:20	N16W153	2425.5
2012 Jul. 23	02:10:07	01:19:07	03:19:45	S17W132	2003.2
2014 Dec. 13	13:57:34	13:06:34	15:07:12	S20W143	2221.6

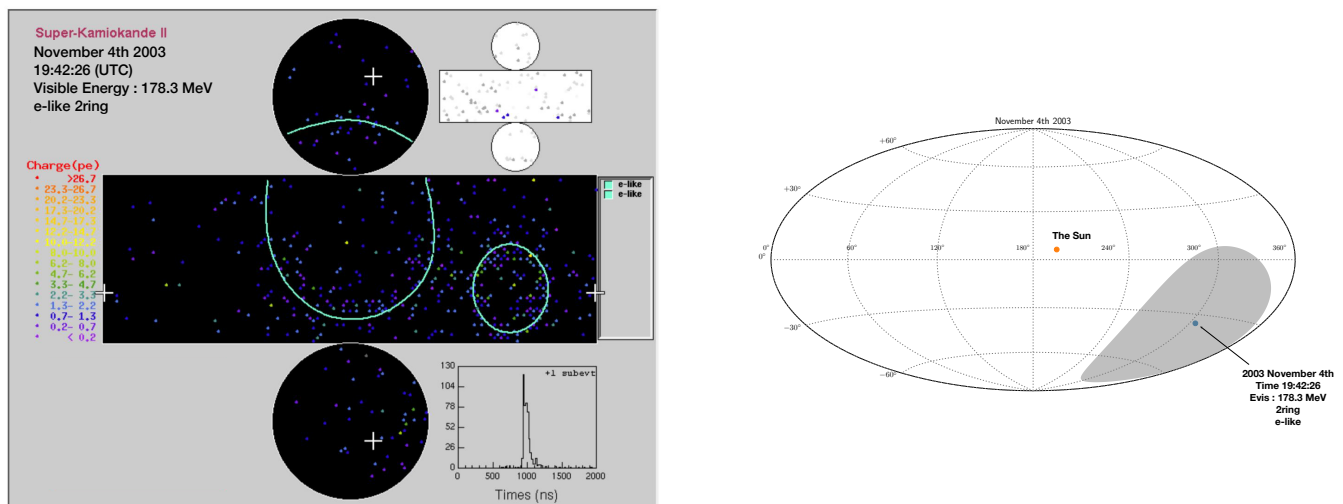


Figure 13. The event display and the sky-map of the observed event within the search window for the solar flare on November 4th, 2003 together with the location of the Sun at that time. The gray contour in the skymap represents the angular resolution for the observed event.

C. EVENT DISPLAY AND SKYMAP OF THE OBSERVED EVENTS FROM SOLAR FLARES ON THE INVISIBLE SIDE

The event displays of neutrino candidates from solar flares on the invisible side and sky maps together with the location of the Sun are shown from Figure 15 to Figure 18.

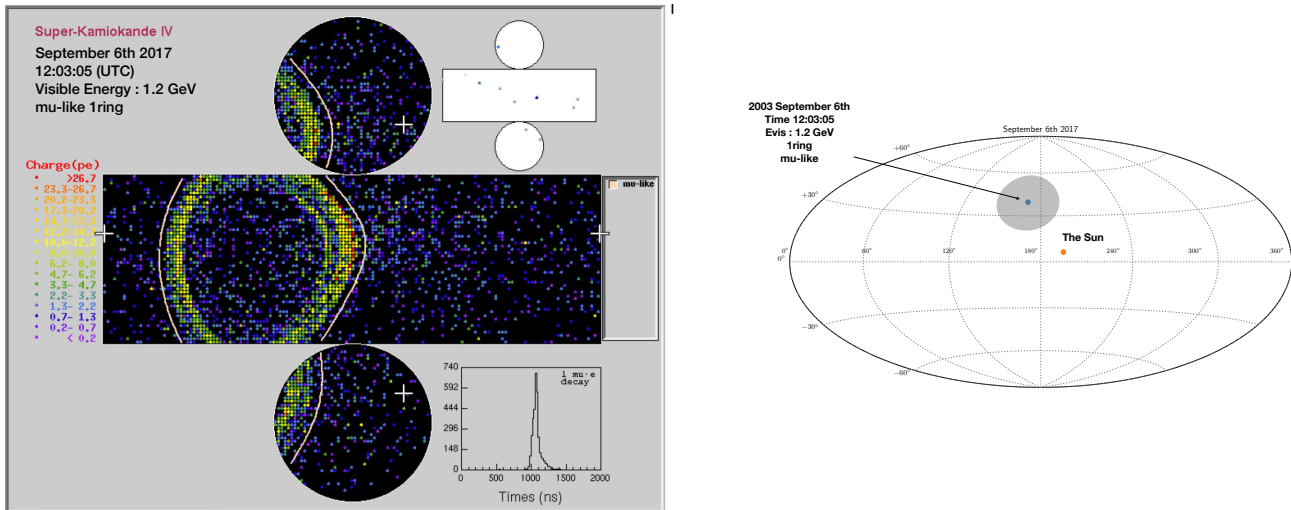


Figure 14. The event display and the sky-map of the observed event within the search window for the solar flare on September 6th, 2017 together with the location of the Sun at that time. The gray contour in the skymap represents the angular resolution for the observed event.

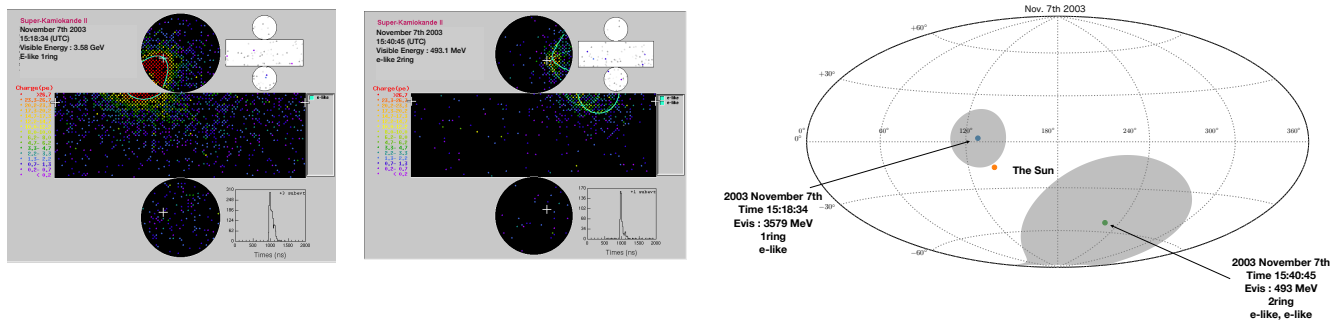


Figure 15. The event displays and the sky-map of the observed events within the search window for the CME occurring on the invisible side of the Sun on November 7th, 2003 together with the location of the Sun at that time. The gray contours in the skymap represent the angular resolutions for each observed event.

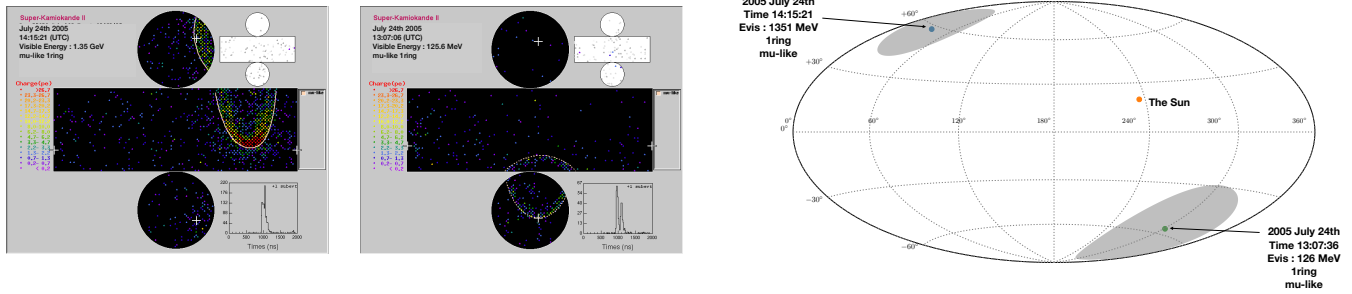


Figure 16. The event displays and the sky-map of the observed events within the search window for the CME occurring on the invisible side of the Sun on July 24th, 2005 together with the location of the Sun at that time. The gray contours in the skymap represent the angular resolutions for each observed event.

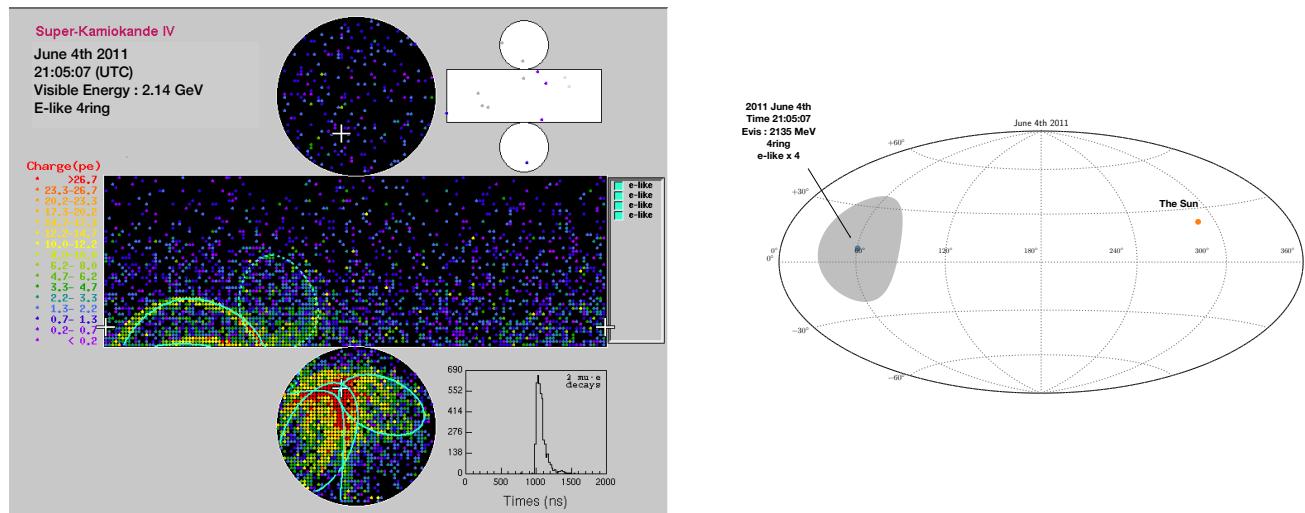


Figure 17. The event display and the sky-map of the observed event within the search window for the CME occurring on the invisible side of the Sun on June 4th, 2011 together with the location of the Sun at that time. The gray contour in the skymap represents the angular resolution for the observed event.

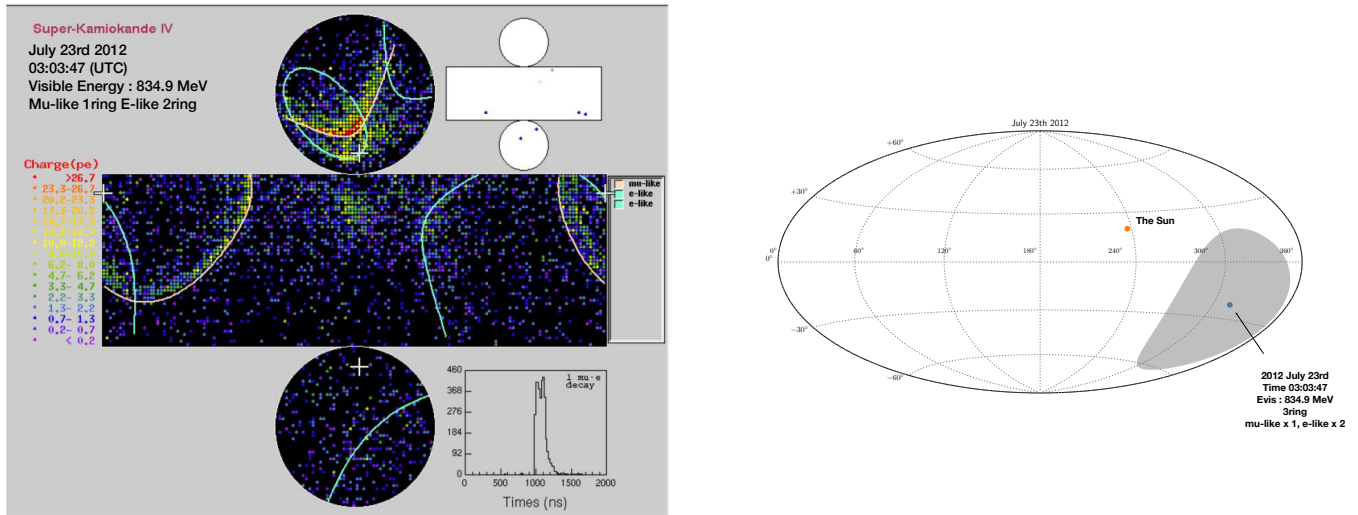


Figure 18. The event display and the sky-map of the observed event within the search window for the CME occurring on the invisible side of the Sun on July 23rd, 2012 together with the location of the Sun at that time. The gray contour in the skymap represents the angular resolution for the observed event.